This is to certify that the

thesis entitled

Spectroscopic Determination of Rotational Temperature in a H_2 Microwave Plasma Flow System and Comparison with Gas Dynamic Temperature

presented by

Randall Chapman

has been accepted towards fulfillment
of the requirements for

M.S. degree in **Chemical Engineering**

Mark C Hanley

Major professor

Date November 27, 1984

SPECTROSCOPIC DETERMINATION OF ROTATIONAL TEMPERATURE IN A HYDROGEN MICROWAVE PLASMA FLOW SYSTEM AND COMPARISON WITH GAS DYNAMIC TEMPERATURE

BY

RANDALL CHAPMAN

A THESIS

Submitted to
Michigan State University
in partial fulfillment of the requirements
for the degree of

MASTER OF SCIENCE

Department of Chemical Engineering

1984

ABSTRACT

SPECTROSCOPIC DETERMINATION OF ROTATIONAL TEMPERATURE
IN A HYDROGEN MICROWAVE PLASMA FLOW SYSTEM
AND COMPARISON WITH GAS DYNAMIC TEMPERATURE

BY

RANDALL CHAPMAN

This thesis develops the theory and illustrates the technique for two different gas temperature measurement methods. Rotational temperatures are determined from intensity measurements of the emission spectra in the visible region for molecular hydrogen. Gas dynamic temperatures are determined from pressure measrements in the hydrogen plasma. The validity of these measrements and their relationship to gas kinetic temperatures are discussed.

Gas temperatures of a flowing hydrogen plasma are presented for flowrates of 10 - 550 sccm, pressures of 1 - 10 torr, and power levels of 250 - 750 W, with a 28 mm I.D. discharge tube. The flow system incorporates a converging-diverging nozzle which results in choked flow conditions with the flowrate and pressure coupled together. The plasma is maintained by a 2.45 GHz microwave generator. The discharge tube is co-axially positioned in a cylindrical resonant cavity which is operated in a TE_{011}^{*} - TM_{111}^{*} mode.

The gas temperatures were found to increase with increasing flowrate (pressure) and with increasing power levels.

TABLE OF CONTENTS

LIST OF TABLES

LIST OF FIGURES

NOMENCLATURE

INTRODUCTION

g_j	statistical weight of j^{th} level
k	Boltzmann's constant
m	mass
u_o	stream velocity
$\bar{v}$	random velocity
$\overline{v^2}$	mean square velocity of the Maxwellian velocity distribution
E_{ave}	average kinetic energy
E_j	energy of the j^{th} level
N	total population
N_j	population of j^{th} level
T_o	stagnation temperature
T_k	kinetic temperature
T_{elec}	electronic temperature
T_{rot}	rotational temperature
T_{vib}	vibrational temperature

EXPERIMENTAL

TE	transverse electric resonant cavity mode
TM	transverse magnetic resonant cavity mode

ROTATIONAL TEMPERATURE

c	speed of light
g	degeneracy
h	Plank's constant
$\hbar$	$h/2\pi$
j	quantum number of the resultant angular momentum for an electron
k	Boltzmann's constant
l	quantum number of the orbital angular momentum for an electron
m	quantum number of the z component of the resultant angular momentum for an electron
m_l	quantum number of the z component of the orbital angular momentum for an electron
m_s	quantum number of the z component of the spin angular momentum for an electron
n	principle quantum number for an electron
s	quantum number of the spin angular momentum for an electron
v	vibrational quantum number, level, or state
A_{nm}	Einstein coefficient for spontaneous emission
E	energy
E	energy level
E_j	energy of j^{th} quantum mechanical state
E_n	energy of n^{th} level
$\bar{E}$	average ensemble energy
$F(J)$	rotational energy term (cm^{-1})
I	quantum number for spin angular momentum for a nucleus
I	spin angular momentum for a nucleus
I_{em}	emission intensity

I_{meas}	measured emission intensity
J	quantum number of the resultant angular momentum for an electron, atom, or molecule
$\mathbf{J}$	resultant angular momentum for an electron, atom, or molecule
J_z	z component of the resultant angular momentum for an electron, atom, or molecule
K	quantum number of the resultant angular momentum, excluding the spin angular momentum of the electrons, for a molecule
$\mathbf{K}$	resultant angular momentum for a molecule, excluding the spin angular momentum of the electrons, for a molecule
L	quantum number of the orbital angular for an electron, atom, or molecule
$\mathbf{L}$	orbital angular momentum for an electron, atom, or molecule
L_z	z component of the orbital angular momentum for an electron, atom, or molecule
M	mechanical property
M	quantum number of the z component of the resultant angular momentum for a molecule
M_n	mechanical propertiy of n^{th} level
M_L	quantum number of the z component of the orbital angular momentum for an atom or molecule
M_s	quantum number of the z component of the spin angular momentum for an atom
$\bar{M}$	average mechanical property
N	population
N_j	population of j^{th} state
N_n	population of n^{th} level
P_n	probability of the n^{th} level
Q	canonical ensemble partition function
Q_{rot}	rotational partition function
R^{ij}	overlap integral between quantum mechanical states i and j
$\|R^{nm}\|^2$	transition probability matrix element
R_λ	instrumental response function
S	quantum number of the spin angular momentum for an electron, atom, or molecule
$\mathbf{S}$	spin angular momentum for an electron, atom, or molecule
S_z	z component of the spin angular momentum for an electron, atom, or molecule
S_J	line strength
T	temperature
T	quantum number of the total nuclear spin angular momentum
$\mathbf{T}$	total nuclear spin angular momentum
T_{rot}	rotational temperature
V	volume
λ	absolute value of the quantum number of the z component of the orbital angular momentum of an electron in a molecule
μ	dipole moment
ν	frequency
Ψ	wave function
Λ	absolute value of the quantum number of the z component of the orbital angular momentum for a molecule
$\mathbf{\Lambda}$	orbital angular momentum along the internuclear axis for a molecule
Σ	quantum number of the z component of the spin angular momentum for a molecule
$\mathbf{\Sigma}$	spin angular momentum along the internuclear axis for a molecule

Ω	quantum number of the total electronic angular momentum along the internuclear axis for a molecule
$\boldsymbol{\Omega}$	total electronic angular momentum along the internuclear axis for a molecule
Ω	microcanonical ensemble partition function

GAS DYNAMIC TEMPERATURE

c	speed of sound
$g(E)$	degeneracy as a function of energy
h	Plank's constant
$\hbar$	$h/2\pi$
k	Boltzmann's constant
m	mass
n	moles
q	individual particle partition function
u	velocity
w	mass flow rate
x	mass fraction
x	mole fraction
z	conversion
A	cross sectional area
C_p	specific heat at constant pressure
$\mathcal{C}_p$	heat capacity at constant pressure
C_v	specific heat at constant volume
$\mathcal{C}_v$	heat capacity at constant volume
E	energy
$\bar{E}$	average ensemble energy
F_o	initial molar flow rate
H	enthalpy/mass
$\mathcal{H}$	enthalpy/mole
I	moment of inertia
M	molecular weight
$\mathbf{M}$	Mach number
N	population
P	pressure
Q	heat/mass
Q	partition function
Q_{rev}	reversible heat/mass
R	gas constant/mass
$\mathcal{R}$	gas constant/mole
S	entropy/mass
$\mathcal{S}$	entropy/mole
T	temperature
T_{gd}	gas dynamic temperature
U	internal energy/mass
$\mathcal{U}$	internal energy/mole
V	volume/mass
$\mathcal{V}$	volume/mole
W	work/mass
W_{rev}	reversible work/mass
γ	ratio of specific heats
θ	characteristic temperature
ν	frequency
ρ	density
ω	angular frequency

ENERGY TRANSFER

w_{air}	cooling air mass flow rate
C_{pair}	specific heat of air
P_{abs}	power absorbed by system
P_{air}	power absrobed by cooling air
P_{gas}	power absorbed by the hydrogen gas as it flows through the system
P_{rad}	power that escapes by radiation
P_{water}	power absorbed by the cooling water
T	temperature of the cooling air
$\%P_{gas}$	the percentage of the power absorbed by the system that is absorbed by the hydrogen gas as it flows through the system

SPECTROSCOPIC DETEMINATION OF ROTATIONAL TEMPERATURE IN A HYDROGEN MICROWAVE PLASMA FLOW SYSTEM AND COMPARISON WITH GAS DYNAMIC TEMPERATURE

Paper prepared for publication

By

Randall Chapman and Martin C. Hawley

Michigan State University

Department of Chemical Engineering

INTRODUCTION

The use of atomic hydrogen as an "in space" rocket propellant has long been considered. The attractive feature of using atomic hydrogen as a fuel is the relatively high recombination reaction energy (104.2 kcal/mole) to low mass ratio. Since the fuel must be first transported into space, the mass of the fuel is a major concern. Presently there is a performance gap between chemical rockets that produce a high thrust density at a low specific impulse and electrostatic ion thrusters that operate at high specific impulses but very low thrust densities. The "free radical" concept has the potential to fill this performance gap (Hawkins, 1981).

Previously proposed concepts have involved the production of the atoms on Earth and their storage aboard the vessel until use. The concept presently being developed involves the on board production of the hydrogen atoms, thereby avoiding the problems associated with free radical storage. The objective of this concept is to convert electrical energy into thrust as efficiently as possible. Electricity provided by solar cells operates a microwave oscillator. Microwave radiation is produced and fed into a resonant cavity. Hydrogen gas is then fed through the cavity where the plasma is formed. Electromagnetic energy is absorbed by the plasma. Simplistically, electrons are accelerated by the electromagnetic fields and transfer their kinetic energy to the neutral and heavy ion constituents via collisions. Dissociation of molecular hydrogen occurs in the plasma. The hydrogen atoms ("free radicals") recombine downstream of the plasma and the gas thermalizes through the vibrational-rotational manifold of the

molecules. The electrical energy has now been transformed into the kinetic energy of the gas which is then expanded through a nozzle to produce thrust.

The focus of this effort was directed towards determining the kinetic energy content of flowing hydrogen gas in a microwave discharge for various experimental conditions. Energy is not a quantity that can be measured directly. However, temperature is an experimental variable that may be measured directly and is thermodynamically related to energy. Temperature is a thermodynamic variable that specifies in part the thermodynamic state of a system. The concept of the temperature of a system is meaningless unless that system is in thermal equilibrium. A system in thermal equilibrium may be described by statistical mechanics.

Each degree of freedom within a system or subsystem that is capable of storing energy may itself be regarded as a system and likewise have a characteristic temperature, providing it is in thermal equilibrium. For an ideal gas, a kinetic temperature, may be defined and is proportional to the average kinetic energy of that gas.

$$E_{ave} = \frac{3}{2} k T_k = \frac{1}{2} m \overline{v^2}$$

where T_k is the kinetic temperature, and $\overline{v^2}$ is the mean square velocity of the Maxwellian velocity distribution. For a flowing gas, a stagnation temperature may be defined and is the temperature which the flowing gas would have if it were adiabatically brought to rest; i.e., if the directed velocity of the particles were randomized. In a gas flowing with a stream velocity, u_o, each particle has a velocity $v + u_o$, where v is the random velocity of that particle.

The stagnation temperature, T_o, is given by

$$T_o = T_k + \frac{m}{3k} u_o^2$$

where T_k is the kinetic or static temperature corresponding to the random velocities. For all gases an electronic temperature may be defined, and for gases consisting of polyatomic molecules, rotational and vibrational temperatures may also be defined. These temperatures are defined by the statistical distribution of the population of the various electronic, rotational and vibrational energy levels of the molecules, via the Maxwell-Boltzmann formula,

$$N_j = \frac{N g_j e^{-E_j/kT}}{\sum_i g_i e^{-E_i/kT}}$$

where N_j is the population of the jth level, g_j is the statistical weight of the jth level, E_j is the energy of the jth level, N is the total population, the sum is over all the electronic, rotational, or vibrational energy levels, and the temperature is then the electronic, rotational or vibrational temperature. There temperatures are designated T_{elec}, T_{rot}, or T_{vib}, respectively. For an ionized gas, there exists ions and free electrons, each of which will likewise have a unique kinetic temperature (Gaydon, 1954).

For a non-flowing system in total thermal equilibrium, all of these temperatures will be the same. For typical laboratory plasmas, such as the plasmas investigated in this study, there are two distinct temperatures. The electrons and ions are accelerated by the electromagnetic fields, however since the electrons are much lighter and

therefore more easily accelerated, the electrons attain a temperature on the order of 10^4 °K. The remainder of the temperatures in the plasma are characteristically on the order of 10^3 °K (Baker, 1961).

In this study, two different temperatures within the plasma were determined by two independent techniques and compared. Rotational temperatures are obtained from spectroscopic measurements and stagnation (gas dynamic) temperatures are obtained from pressure measurements. These methods have two distinct advantages; the measurements do not interfere with the steady state operation of the experiment and can be taken simulataneously.

EXPERIMENTAL

I. H_2 Flow System

The diagram of the hydrogen flow system is shown in Figure 1. Hydrogen gas from a storage cylinder was fed through 1/4 in. stainless steel tubing, through the flow meter to the variable leak valve. A pressure regulator at the outlet of the storage cylinder controlled the pressure to the valve. The pressure drop across the valve was large so that small fluctuations upstream of the valve did not effect the downstream pressure. The hydrogen gas then flowed from the valve through 1/4 in. stainless steel tubing and flexible stainless steel tubing to the discharge tube. The hydrogen gas then flowed through the discharge tube and rubber vacuum hose to a vacuum tank. The vacuum tank was maintained at a background pressure of about 10^{-5} torr. The flow meter was a Hastings mass flow rate meter. It was calibrated for hydrogen and had a range of 0-500 sccm.

The discharge tube was a convering-diverging venturi fabricated from fused quartz. The details of the discharge tube are shown in Figure 2. The discharge tube was placed co-axially inside the cylindrical resonant cavity, with the nozzle positioned 5 mm before the exit of the cavity. The plasma was formed upstream of the nozzle. The discharge tube had a cooling air jacket, as seen in Figure 2. Cooling air was delivered at a constant rate of 3.7 g/sec and its temperature at the exit of the cooling air jacket was monitored with an iron-constantan thermocouple. The cooling-air was required to maintain steady state boundary conditions, i.e., wall temperature of the plasma, and to prevent the discharge tube wall from melting or being reduced through reactions with atomic hydrogen. The direction of the

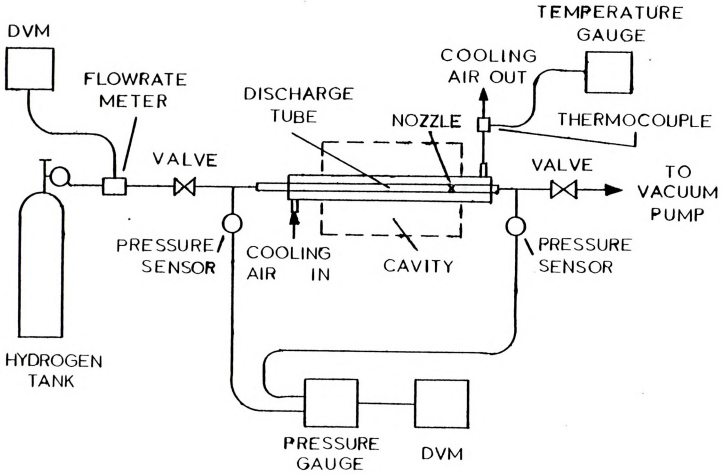

Figure 1. Hydrogen flow system diagram.

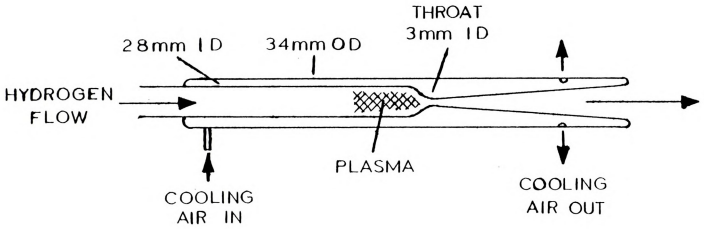

Figure 2. Discharge tube diagram.

cooling air flow was co-current with the hydrogen gas flow. The discharge tube was coated with dri-film to reduce the wall recombination reaction of the hydrogen atoms.

The discharge tube was connected to the flow system via Veeco fittings. This facilitated changing tubes and provided an ideal location for pressure taps. Pressure taps were positioned upstream and downstream of the discharge tube. The pressure was measured by Datametric Barocel capacitance-type pressure sensors with a range of 10^{-3} - 10^{3} torr.

Since the nozzle in the discharge tube was the only flow restriction downstream of the flow meter and variable leak valve, and since that restriction was fixed, the flow rate and pressure in the discharge region were coupled together. The coupling of the flow rate and pressure was required for the gas dynamic measurements to be discussed later.

II. Microwave Power System

The diagram of the microwave power system is shown in Figure 3. The microwave power was generated by a Raytheon PGH-100 magnetron. This source was filtered and had a continuously variable output of 280-730 W at a fixed frequency of 2.45 GHz. The microwaves were directed through rigid rectangular waveguide to a water cooled isolator. The isolator was required to protect the magnetron from reflected power. The microwaves were then fed through a 40-dB dual directional coupler. The directional coupler allowed for the measurement of incident and reflected power levels. The incident power level was measured with a 435-A Hewlett-Packard power meter. The reflected power level was measured with a 436-A Hewlett-Packard power meter that has an auto-range feature which was convenient when tuning the cavity. Both meters used 100 μW thermocouple power sensors.

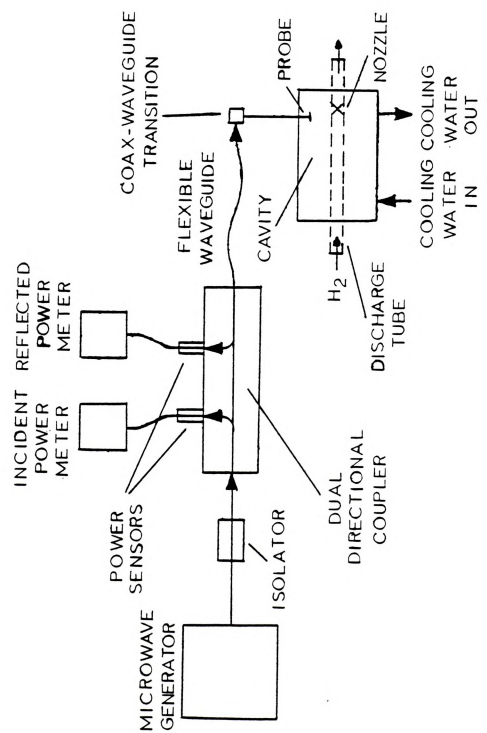

Figure 3. Microwave power system diagram.

The dual directional coupler and power meters were calibrated with a known input power at the operating frequency of 2.45 GHz. The microwaves were then fed through a section of flexible waveguide to a waveguide to coax transition. A coaxial excitation probe was connected to this transition and inserted into the cylindrical resonant cavity. The section of flexible waveguide was required so that the depth at which the probe was inserted into the cavity could be continuously variable. The details of the plasma cavity are given in Figure 4. The screened window allowed for viewing of the plasma and spectroscopic diagnostics. The cavity was water cooled to maintain steady state bondary conditions, i.e., wall temperature, and to prevent damage to the cavity.

A solution to Maxwell's equations for the cavity yields a characteristic equation involving the plasma characteristics, the cavity geometry and the driving frequency (Jackson, 1975). The solutions for this equation are quantized and the cavity is capable of supporting many modes. Since the driving frequency and cavity diameter were fixed, the different operating modes were obtained by changing the cavity length. The length of the cavity was determined by the position of the sliding short and was continuously variable from 6 to 14 cm.

The simplest description of a plasma is the "Cold Plasma Model", with the important plasma characteristic being the electron density (Krall, 1973). The "Cold Plasma Model" is sufficient for the level of treatment involved in this work. Since the plasma diameter is small compared to the cavity diameter, the plasma only slightly perturbs the empty cavity resonant conditions. The important distinction between solutions for the empty cavity and for a cavity containing a plasma is that with the plasma present, pure TE and TM, transverse electric and

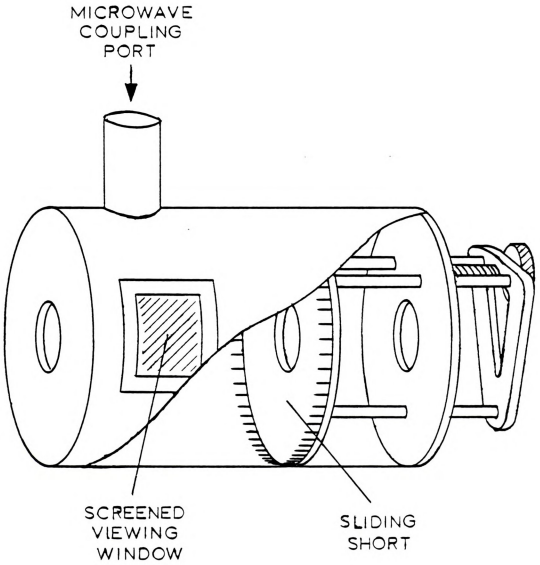

Figure 4. Plasma cavity diagram.

magnetic, solutions are no longer possible. To satisfy the boundary conditions, both the TE and TM solutions are required so that the solutions for the cavity with the plasma involve TE* and TM* hybrid modes.

The adjustable probe depth and sliding short length provide the means with which to optimally tune the cavity. As the plasma conditions change, the probe depth and sliding short length were adjusted to achieve the resonant condition of minimum reflected power.

III. Spectroscopic Diagnostic System

The diagram of the spectroscopic diagnostic system is shown in Figure 5. The emission from the plasma was monitored by a McPherson 216.5 Spectrometer which had a focal length of 0.5 m, a spectral range of 1050-5000 Å, and a diffraction grating with 2400 G/mm with a resolution better than 0.5 Å. The entrance slit to the spectrometer was set for a slit height of 20 mm and a slit width of 5 μm. The optimum slit settings were determined by trial and error, and remained constant for the entire experimental investigation. The spectrometer was placed as close as physically possible to the discharge to obtain the greatest emission intensity possible. The distance from the discharge to the entrance slit was 30 cm.

The utilization of an optical lens system was considered. The lens system should optimize the emission intensity illuminating the spectrometer, thereby improving the signal to noise ratio, also it would enable measurements to be obtained as a function of distance along the discharge, i.e., axial resolution. The spectra obtained using the lens system were qualitatively different than those obtained without the lens system, however the signal to noise ratio was not greatly improved. The gas dynamic measurements that were used as a comparison with the spectroscopic measurements, yield a "bulk"

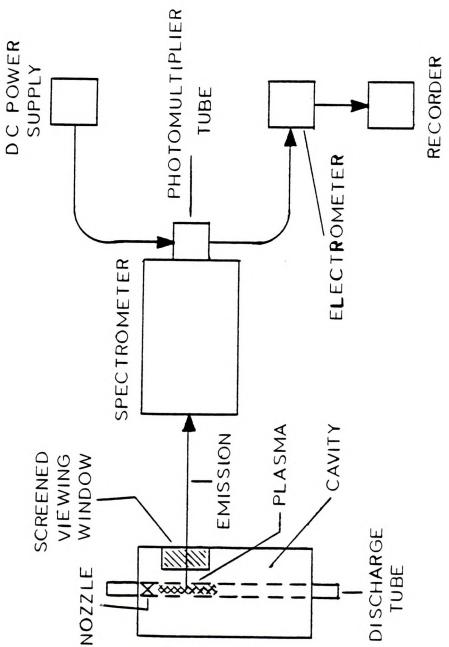

Figure 5. Spectroscopic diagnostic system diagram.

measurement, i.e., spatial averaged over the entire discharge. Also, the dri-film coating on the discharge tube became non-uniformly discolored with age. From these considerations, the decision was made to forego the use of the lens system and obtain "bulk" measurements.

The spectrometer employed a RCA 4840 photomultiplier tube to measure the light intensity, the PMT required on operating voltage of 1000 V which was provided by a Harrison 6110A D.C. power supply. The current produced by the PMT was monitored by a Kiethley 616 electrometer which was connected to a Honeywell 195 Electronik Recorder to provide the spectra.

The emission intensity had a strong dependence on the discharge pressure. Within the pressure range of this experimental investigation, 1-10 torr, the intensity decreased with increasing pressure. The signal to noise ratio of this experimental apparatus determined the uncertainty of the spectroscopic measurements. The signal to noise ratio was found to originate from two major sources; the microwave power generator and the PMT.

Fluctuations in the power output of the microwave generator gave rise to visible fluctuations in the emission intensity of the discharge. The fluctuations of the microwave generator may have been power level and/or frequency fluctuations. The percent of noise due to the microwave generator seemed to be mainly dependent on the emission intensity and increased with decreasing intensity. At the conditions for the largest signal to noise ratio, 50% of the noise was due to the microwave generator.

The other major source of noise came from the PMT. Every PMT has a characteristic dark current due to the thermal excitation of electrons within it. Since this is a random process, there is an inherent noise associated with the dark current. The dark current and its inherent noise decreases with decreasing PMT temperatures. In an

attempt to improve the signal to noise ratio, a cooling shroud was placed over the PMT and cooled with liquid nitrogen. This reduced the noise due to the PMT. However, since the PMT was not the major source of noise at the conditions where the noise was the most detrimental, the cooling of the PMT was only moderately successful and hence abandoned.

The noise due to the PMT comprised 50% of the total noise at low pressures and decreases for increasing pressure. An upper limit of 10 torr for this investigation was established since the uncertainties of the measurements at pressures greater than 10 torr became so large that they rendered the data meaningless.

IV. Experimental Procedure

Once the experimental apparatus was assembled, a vacuum was constantly maintained within the system. This was to reduce contamination of the flow system by air, inparticularly the dri-film coated discharge tube. Since the flow rate and pressure in the discharge region were coupled together and the pressure was the quantity required in the gas dynamic measurements; the experimental data was obtained as a function of power applied to the plasma cavity for a given hydrogen mass flow rate. Of course as the power increased, the temperature and pressure in the discharge region increased, since the mass flow rate is held constant. A pressure range for this experimental investigation of 1-10 torr was chosen. A simplistic model derived from the Langevin equation assuming a momentum transfer collision frequency for hydrogen of $4.85 \times 10^9 \times P$ (P in torr) (Brown, 1966) yields a maximum in the absorbed power of the plasma for a driving frequency of 2.45 GHz at a pressure of 3.2 torr (Cherrington, 1979). Since it was desired to obtain experimental information that bracketed 3.2 torr, and the spectroscopic diagnostic technique had an upper limit of 10 torr, a lower limit of 1 torr was arbitrarily

chosen. Hence, hydrogen mass flow rates of 13.1, 86.8, 261.6 and 544.6 sccm which corresponded to about 1, 3, 6, and 10 torr respectively, were established for the investigation.

All of the experimental data was obtained for a sliding short length of about 8.8 cm. A plot of sliding short length as a function of plasma frequency for various cavity modes shows an intersection of the TE^*_{011} and TM^*_{111} modes in the region corresponding to the experimental conditions of the investigation (Mallavarpu, 1976). Therefore the cavity mode can not be completely determined and was considered to be some combination of the TE^*_{011} and TM^*_{111} modes.

Prior to operation of the system, all electronic equipment was switched on and allowed to warm up; also, the cooling water and air sources were opened and the streams were allowed to reach steady state conditions. The power meters and pressure gauges drifted from zero and needed to be periodically re-zeroed. To run the experiment, hydrogen gas was introduced into the system at the desired flowrate. The microwave power was then applied to the cavity at the desired power level. The cavity was then tuned by adjusting the probe depth and sliding short length to obtain a minimum in the reflected power level, i.e., to obtain a best match between the magnetron and the plasma cavity load. Usually as the cavity was approaching a match the plasma self-ignited. As the conditions in the plasma change, the cavity had to be continuously retuned. Through trial and error, the plasma reached steady state conditions with the cavity tuned to a best possible match. At steady state conditions, the reflected power was always less than 1% of the incident power. Once steady state conditions were achieved in the system, a data point could then be taken. The system remained at steady state indefinitely, however a change in

any of the experimental parameters required the system to be retuned and a set of new steady state conditions reached.

A reference set of data was taken that gave the pressure upstream and downstream of the discharge region; i.e., the nozzle, as a function of the mass flow rate of the hydrogen gas stream without power being applied to the plasma cavity. The reference data was required for the gas dynamic measurements.

ROTATIONAL TEMPERATURE

I. Theoretical Background

Quantum mechanics describes matter as existing in discrete energy states (Schiff, 1968). The connection between the quantum mechanical energy states available to an N-body system and its thermodynamic properties is made through statistical mechanics and the partition function (McQuarrie, 1973). The definitions of the non-mechanical thermodynamic properties involve the concept of temperature.

An ensemble is a collection of a very large number of systems each of which is constructed to resemble, on a macroscopic level, the thermodynamic system of interest. The microcanonical ensemble is an ensemble in which N, V, and E for each system is fixed. The number of quantum mechanical energy states available to each system is the microcanonical ensemble partition function, Ω (N,V,E). This is also the degeneracy, g, of the system.

The canonical ensemble has N, V, and T fixed, for each system. The canonical ensemble partition function is given as

$$Q(N,V,T) = \sum_j e^{-E_j(N,V)/kT}$$

where the sum is over all the quantum mechanical states, j, available to each system, E_j is the quantum mechanical energy of each state, and k is the Boltzmann constant.

From the microcanonical ensemble, it is seen that there are Ω(N,V,E) quantum mechanical energy states available to the particles for each energy level, E. The canonical ensemble partition function can then be summed over the energy levels, E, instead of the energy states, j.

$$Q(N,V,T) = \sum_{E} \Omega(N,V,E)\ e^{-E(N,V)/kT}$$

In other notation, this is written

$$Q = \sum_{n} g_n\ e^{-E_n/kT}$$

where n designates the energy level.

The probability, P_n, that a system will be in the energy level n is

$$P_n = \frac{g_n\ e^{-E_n/kT}}{Q}$$

A system of atoms or molecules initially in an excited energy level E_n, may fall to a lower energy level, E_m, spontaneously with the emission of electromagnetic radiation. This energy difference is given by

$$E_n - E_m = h\nu_{nm}$$

where h is Plank's constant and ν_{nm} is the frequency of the emitted radiation. The number of particles, N_n, in the energy level n is given by

$$N_n = N\ P_n = \frac{N\ g_n\ e^{-E_n/kT}}{Q}$$

where N is the total number of a particle in the system. This result is known as the Maxwell-Boltzmann distribution law. The ensemble average of any mechanical property, M, is given by

$$\bar{M} = \sum_{n} M_n P_n$$

Thus

$$\bar{E} = \sum_n E_n P_n = \frac{\sum_n E_n g_n e^{-E_n/kT}}{Q} = kT^2 \left(\frac{\partial \ln Q}{\partial T}\right)_{N,V}$$

is the average energy of the system and corresponds to the dynamic energy E.

Spontaneous emission is a random process that results in radiation that is isotropic and incoherent (Herzberg, 1950). The intensity of the electromagnetic radiation spontaneously emitted by a sample is given by

$$I_{em}^{nm} = N_n h\nu_{nm} A_{nm}$$

where the intensity has units of energy/sec, N_n is the population of particles in the initial level, n, and A_{nm} is the Einstein coefficient for spontaneous emission.

Using the Maxwell-Boltzmann distribution law

$$I_{em}^{nm} = \frac{N g_n h\nu_{nm} A_{nm}}{Q}$$

The Einstein coefficient for spontaneous emission, A_{nm}, is the probability per unit time that a particle in the upper energy level, n, will undergo a transition to the lower energy level, m, spontaneously. An expression for the Einstein coefficient may be obtained from quantum mechanical considerations. The interaction between electromagnetic radiation and matter involves one or more terms of the multiplole expansion of the atomic or molecular system. For radiation resulting from eletric dipole type transmition, which is of interest in this study, the Einstein coefficient is given by

$$A_{nm} = \frac{64\pi^4 \nu_{nm}^3}{3hc^3 g_n} |R^{nm}|^2$$

where c is the speed of light and $|R^{nm}|^2$ is the transition probability matrix element.

$$|R^{nm}|^2 = \sum |R^{ij}|^2$$

where the summation is over all the possible combinations of the degenerate states i(j) in the level n(m).

$$R^{ij} = \int \Psi_i^* \mu \Psi_j \, d\tau = \langle i|\mu|j\rangle$$

where μ is the electric dipole moment and Ψ is the wave function of the state i or j, which satisfies the Schrodinger equation.

Spontaneous emission occurs for a transition between two levels that yield a non-zero transition probability matrix element. The restrictions on the wave functions between the two levels which allow for a non-zero transition matrix element are called the selection rules. The intensity of the spontaneous radiation emitted by an electric type dipole is then

$$I_{em}^{nm} = \frac{64\pi^4 \nu_{nm}^4 N}{3c^3 Q} |R^{nm}|^2$$

The energy state of an atomic system is determined from its electronic structure. Each electron in the system is completely characterized by a set of four quantum numbers; n, l, m_l, and m_s. The principal quantum number, n, refers to the energy level in which the

electron resides, $n = 0,1,2,3\cdots$. The orbital angular momentum quantum number, l, has allowed values, $l = 0,1,2,\cdots,n-1$. The magnitude squared of the orbital angular momentum is given by

$$L^2 = l(l+1)\,\hbar^2$$

where $\hbar = \frac{h}{2\pi}$

The orbital angular momentum, L, is a constant of the motion. The quantum number for the space quantization of the orbital angular momentum, m_l, has allowed values, $m_l = 0,\pm1,\pm2,\cdots,\pm l$.

The angle that L makes with the z axis is not arbitrary, the z component of L is quantized and given by

$$L_z = m_l\hbar$$

The spin angular momentum quantum number, m_s, has allowed values, $m_s = \pm 1/2$. The z component of the spin angular momentum is given by

$$S_z = m_s\hbar$$

The magnitude squared of the spin angular momentum is given by

$$S^2 = s(s+1)\,\hbar^2 = \frac{3}{4}\,\hbar^2$$

where $s = 1/2$.

The resultant angular momentum, J, is the vector sum of the orbital and spin angular momentum.

$$J = L + S$$

As with L and S, the magnitude squared and z component of J are given by

$$J_2 = j(j+1)\,\hbar^2$$

$$J_z = L_z + S_z = m\hbar$$

where j is the resultant angular momentum quantum number, $j = l \pm 1/2$ and m is the sum of the z components of the orbital and angular momenta,

$$m = m_l + m_s = \pm j, \pm(j-1), \cdots$$

The letters s, p, d, f, $\cdots$ are used to designate the values for $l = 0,1,2,3,\cdots$. The total resultant, J, orbital, L, and spin, S, angular momenta for the atomic system, and their z components are obtained from summing over each electron, i, in the system.

$$\mathbf{L} = \sum_i \mathbf{L}_i$$

$$\mathbf{S} = \sum_i \mathbf{S}_i$$

$$\mathbf{J} = \sum_i \mathbf{J}_i = \mathbf{L} + \mathbf{S}$$

$$L_z = \sum_i L_{z_i} = M_L \hbar$$

$$S_z = \sum_i S_{z_i} = M_S \hbar$$

$$J_z = \sum_i J_{z_i} = L_z + S_z = M\hbar$$

The magnitude squared of the total angular momenta are given by

$$J^2 = J(J+1)\,\hbar^2$$

$$L^2 = L(L+1)\,\hbar^2$$

$$S^2 = S(S+1)\,\hbar^2$$

where J, L and S are now the total resultant, orbital and spin angular momenta quantum numbers for the atomic system. The state of the

atomic system is characterized by a set J, L, and S, of quantum numbers, where

$$J = L+S,\ L+S-1,\ \cdots,\ |L-S|$$

States with the same L and S value constitute an L-S term. They have practically the same energy and are called a multiplet. There are 2S+1 states with different J values in an L-S term. That number is called ther multiplicity of the term. The letters S, P, D, F, $\cdots$ are used to designate the values for L = 0,1,2,3,$\cdots$. The energy state of the atomic system is then represented as

$$n\mathit{l}^{2S+1}L_J$$

where n and l refer to the electron in the highest electronic state within the system.

The selection rules obtained from the transition probability matrix elements for electric dipole type transitions are

$\Delta L = \pm 1$, $\Delta S = 0$

$\Delta J = 0, \pm 1$ with $J_n=0 \not\leftrightarrow J_m=0$

$\Delta M = 0, \pm 1$

Here, Δ takes on the meaning of the quantum number of the upper (higher) energy state, E', minus that of the lower energy state, E"; not necessarily the initial, E_n, and final, E_m, energy states. The exclusions of $J_n = 0 \rightarrow J_m = 0$ transition results from the fact that a proton possesses angular momentum. Also $\Delta M = 0$ is not possible in a $\Delta J = 0$ transition.

The selection rules for the electron residing in the highest energy state are

$$\Delta n = 1,2,3,\cdots$$

$$\Delta \mathit{l} = \pm 1$$

The simplest and most extensively studied atomic system is the hydrogen atom. The ground state of the hydrogen atom is found to be $1s^2S_{1/2}$. The set of transitions terminating in the ground state are given by

$$np^2P_{3/2,1/2} \rightarrow 1s^2S_{1/2}$$

where $n > 1$.

These transitions emit radiation in the U.V. region and the resulting spectral lines are called the Lyman series.

The set of transitions terminating in the first excited state are given by

$$nd^2D_{3/2,1/2} \rightarrow 2p^2P_{3/2,1/2}$$

where $n > 2$.

These transitions emit radiation in the visible red region and the resulting set of spectral lines is called the Balmer series.

The experimental apparatus was set up only to obtain spectra in the visible region. Typically, the Balmer series lines are the most intense lines in the visible region and are primarily responsible for the red color that is characteristic of hydrogen plasmas. Spectra of the Balmer lines were obtained during this study, but no effort was made to get quantitative results from them.

Determination of the energy state of a molecular system is more complicated than in the atomic case. Since the electrons no longer move in a central field of force, the orbital angular momentum of each election is not a constant of the motion. In the case of diatomics, the internuclear axis is defined as the z-axis. The z component of the orbital angular momentum of each election is then a constant given by

$$L_z = m_l h$$

where $m_l = 0,\pm1,\pm2,\cdots$, similar to the atomic system case. Since the sign of m_l determines the sense of rotation of the electron about the internuclear axis, and the energy of the electron is independent of the sense of rotation; the quantum number of interest is defined as $\lambda = |m_l|$. The symbols σ, π, δ, ϕ, $\cdots$ are used to designate the numerical values of $\lambda = 0,1,2,3,\cdots$ ($m_l = 0,\pm1,\pm2,\pm3,\cdots$). The z component of the total orbital angular momentum, L_z, for the molecular system is obtained from summing over the electrons in the system

$$L_z = \sum_i L_{z_i}$$

$$= \sum_i m_{l_i} \hbar$$

$$= M_L \hbar$$

where $M_L = \sum_i m_{l_i}$

The energy state of the electrons in a molecular system is then characterized by Λ, where $\Lambda = |M_L|$. The symbols Σ, Π, Δ, Φ, $\cdots$ are used to designate the numerical values of $\Lambda = 0,1,2,3,\cdots$. Since for every value of $\Lambda > 0$, there are two values of M_L, the states Π, Δ, Φ, $\cdots$ are said to be doubly degenerate.

Designation of the spin angular momentum states for the electrons in the molecular system is similar to that of an atomic system.

As in the atomic case, the total spin angular momentum and its z component are obtained by summing over the individual electrons. In the molecular case, M_s is denoted by Σ.

$$S = \sum_i S_i$$

$$S_z = \sum_i S_{z_i}$$

$$= \Sigma \hbar$$

the magnitude squared of S is given by

$$S^2 = S(S+1)\,\hbar$$

where S is the spin angular momentum quantum number of the molecular system.

For molecular states with $\Lambda \neq 0$, there exists a magnetic field along the internuclear axis which causes a precession of S about that axis and results in 2S+1 possible values for Σ.

$$\Sigma = S,\ S-1,\ S-2,\ \cdots,\ -S$$

For molecular states with $\Lambda=0$, Σ is not defined.

The total electronic angular momentum along the internuclear axis is denoted by Ω. Ω is analogous to J for the atomic case, however, Ω, Λ, and Σ are all directed along the internuclear axis. The resultant electronic angular momentum quantum number, Ω, is then given by

$$\Omega = |\Lambda+\Sigma|$$

The symmetry properties of the electronic eigenfunction are important. An electronic wave function of a non-degenerate state, Σ, that changes sign when reflected at any plane through the internuclear axis is designated Σ^-, and a wave function that remains unchanged is designated Σ^+. Non-degenerate states with different symmetry wave functions have different energies. Degenerate states with different symmetry wave functions have exactly the same energies and the symmetry distinction becomes meaningless. However, it will be seen later that this degeneracy is removed by the inclusion of molecular rotation. For diatomics with nuclei of like charge, there exists a center of symmetry on the internuclear axis between the two nuclei.

Electronic wave functions that change signs when reflected about the center are designated u and wave functions whose signs remain unchanged are designated g.

In the case where the molecular electronic state closely resembles an atomic state, the electronic energy state is given as

$$n\mathit{l}^{2S+1}\Lambda$$

where n and l are the quantum numbers associated with the electron in the highest energy state within the atom.

In the case where the molecular electronic state differs from an atomic state, the electronic energy state is given as

$$X^{2S+1}\Lambda$$

where X corresponds to the eletronic molecular orbital state of the molecule. X is the ground state; B,C,D,$\cdots$ are excited states.

In the cases where they apply, the parity of the electronic eigenfunction is given as a superscript and the symmetry of the electronic eigenfunction is given as a subscript.

The ground state of the hydrogen molecule is $1s^1\Sigma$. The potential energy curves for various electronic states of the hydrogen molecule are given in Figure 6 (Sharp, 1971). Electronic transitions of molecular hydrogen ending in the ground state are the Lyman bands

$$np^1\Sigma \rightarrow 1s^1\Sigma \qquad n > 1$$

and the Werner bands

$$np^1\Pi \rightarrow 1s^1\Sigma \qquad n > 1$$

both of which radiate in the U.V. region.

The selection rules for an electronic transition are

$$\Delta\Lambda = 0, \pm 1$$

$$\Delta S = 0$$

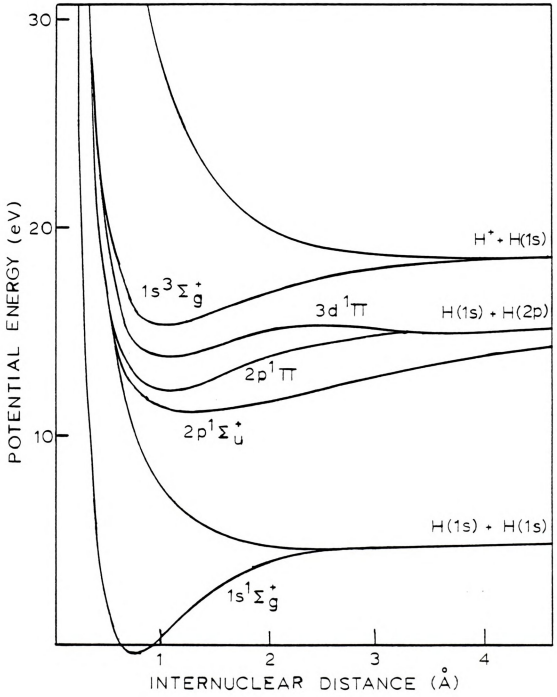

Figure 6. Potential energy curves for hydrogen.

and that Σ^+ states can not combine with Σ^- state, which is denoted

$$\Sigma^+ \nleftrightarrow \Sigma^-$$

or $$\Sigma^+ \leftrightarrow \Sigma^+$$

$$\Sigma^- \leftrightarrow \Sigma^-$$

and for molecules with nuclei of equal charge, even states can only combine with uneven states

$$g \leftrightarrow u$$

or $$g \nleftrightarrow g$$

$$u \nleftrightarrow u.$$

Again, the selection rules for the electron residing in the highest energy state

$$\Delta n = 1,2,3,\cdots$$

$$\Delta l = \pm 1$$

Likewise, the selection rules for the electronic molecular orbitals

$$B,C,D,\cdots \leftrightarrow X$$

$$C,D,E,\cdots \leftrightarrow B$$

$$D,E,F,\cdots \leftrightarrow C$$

$$\vdots$$

The hydrogen molecule is one of the simplest and the most extensively studied molecule. Specification of the electronic state does not completely characterize the energy state of a molecule. The designation of an electronic molecular state has assumed that the two nuclei are space-fixed. Complete characterization of the molecular energy state requires specification of the vibrational and rotational energy states. The vibrational motion of the molecule is treated as an oscillation of the nuclei along the internuclear axis. A vibrational energy state within an electronic state is characterized by the

vibrational quantum number, $v = 0,1,2,3,\cdots$. The interactions of the electronic and vibrational motions is taken into account as the vibrational levels are chosen to fit the potential energy curve of the electronic state, which is a function of internuclear distance.

Figure 7 shows that the energy spacing between adjacent vibrational levels decreases as the vibrational quantum number increases, and that they are much smaller than the energy spacing between electronic states. A transition between two vibrational states is designated as $(v_n - v_m)$, where the v_n indicates the vibrational level of the initial energy state and the v_m indicates the vibrational level of the final energy state. Symmetry considerations of vibrational levels are meaningless as the vibrational eigenfunctions depend only on the internuclear distance. The vibrational levels are non-degenerate.

The rotational motion of the molecule is treated as a rotation of the molecule as a whole about an axis through the center of mass perpendicular to the internuclear axis. The nuclear rotational angular momentum, **N**, results from this motion. The corresponding quantum number is denoted by N, where $N = 0,1,2,3,\cdots$. The different angular momenta in the molecule, **S**, **L**, and **N**, always form a resultant total angular momentum, **J**. The rotational state within a vibrational state within an electronic state is characterized by the corresponding quantum number J, where

$$J = J_{min}, J_{min} + 1, J_{min} + 2, \cdots$$

Figure 8 shows how these energy levels are nested.

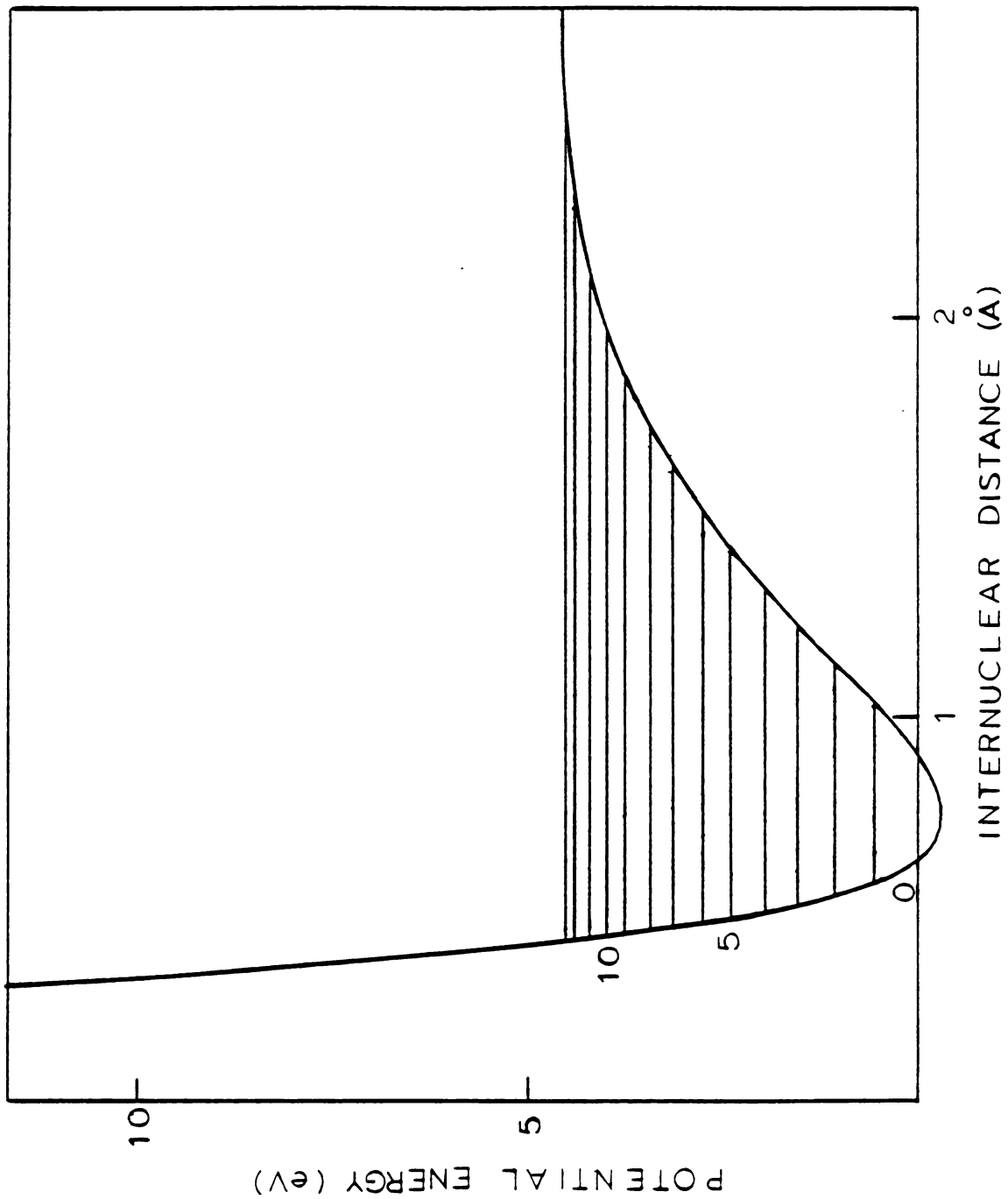

Figure 7. Vibrational energy levels of the $1s^1\Sigma_g^+$ state.

Figure 8 shows that the energy spacing between adjacent rotational levels increases as the rotational quantum number increases, and that they are much smaller than the energy spacing between the vibrational levels.

The selection rule for a rotational transition is $\Delta J = 0, \pm 1$ with the restriction $J = 0 \not\leftrightarrow J = 0$. The 3 possibilities arising from this selection rule are called branches.

$\Delta J = +1$	R Branch
0	Q Branch
-1	P Branch

A single rotational transition (line) shown in Figure 9, is labeled by the branch and the rotational quantum number in the lower energy state, i.e., R(J"), P(J") or Q(J").

Vibrational transitions (bands) radiate in the I.R. region and the rotational transitions make up the fine structure of these bands. Homonuclear the molecules do not have a permanent electric dipole moment and therefore do not radiate in this region. However, electronic transitions of homonuclear molecules involve an electric dipole moment and radiate in the U.V.-visible region. The individual lines seen in this case are the rotational lines of a vibrational band in an electronic transition.

The simplest model used to describe the rotation of a diatomic molecule is the rigid rotor approximation. This treatment views the molecule as having a fixed internuclear distance. The molecule resembles a rigid dumbell. In this model, the angular momentum of the molecule is perpendicular to the internuclear axis, i.e., $\Lambda = 0$. The symmetric top model allows for the angular momentum of the molecule to

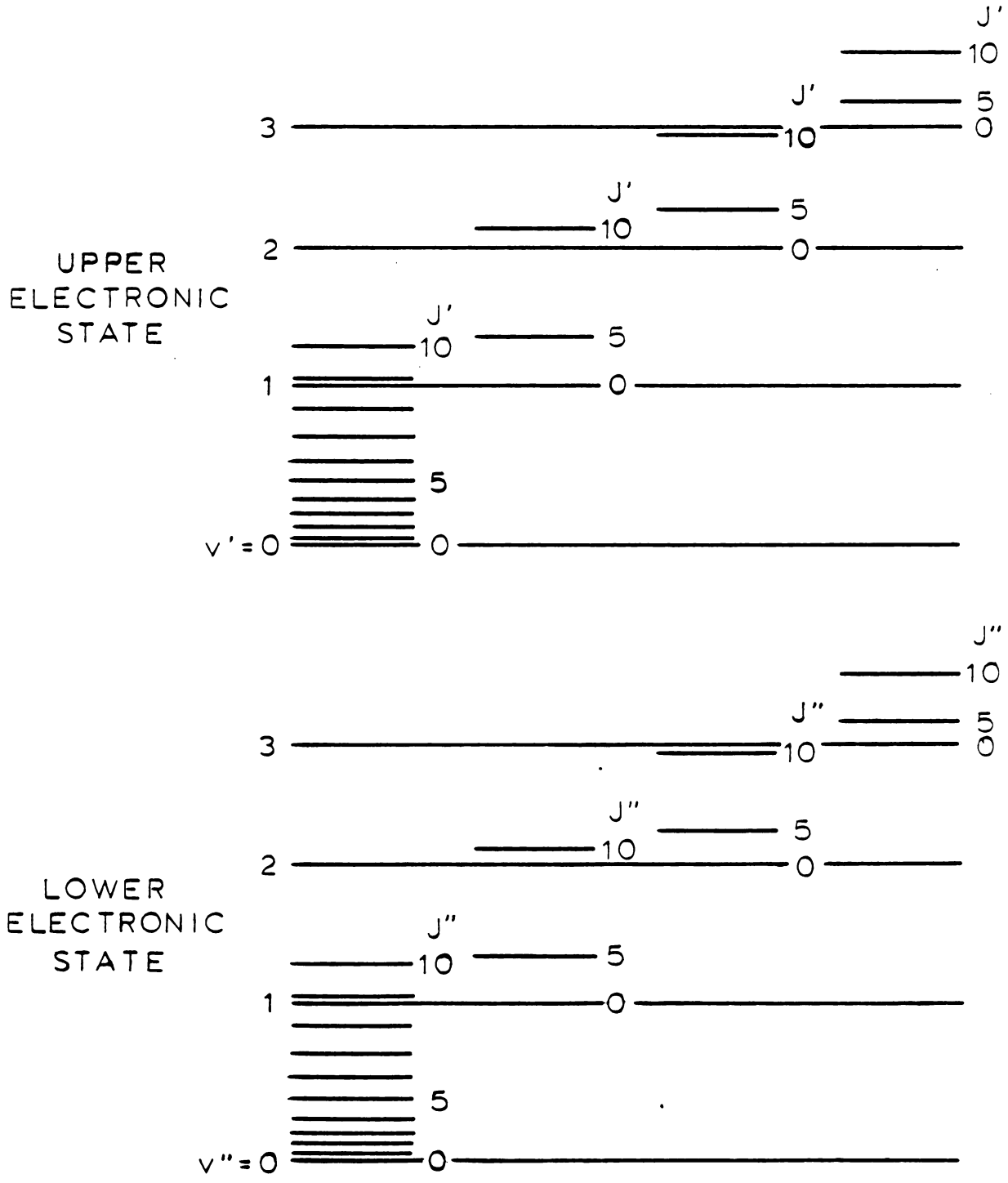

Figure 8. Rotational energy levels of an arbitrary vibrational and electronic state.

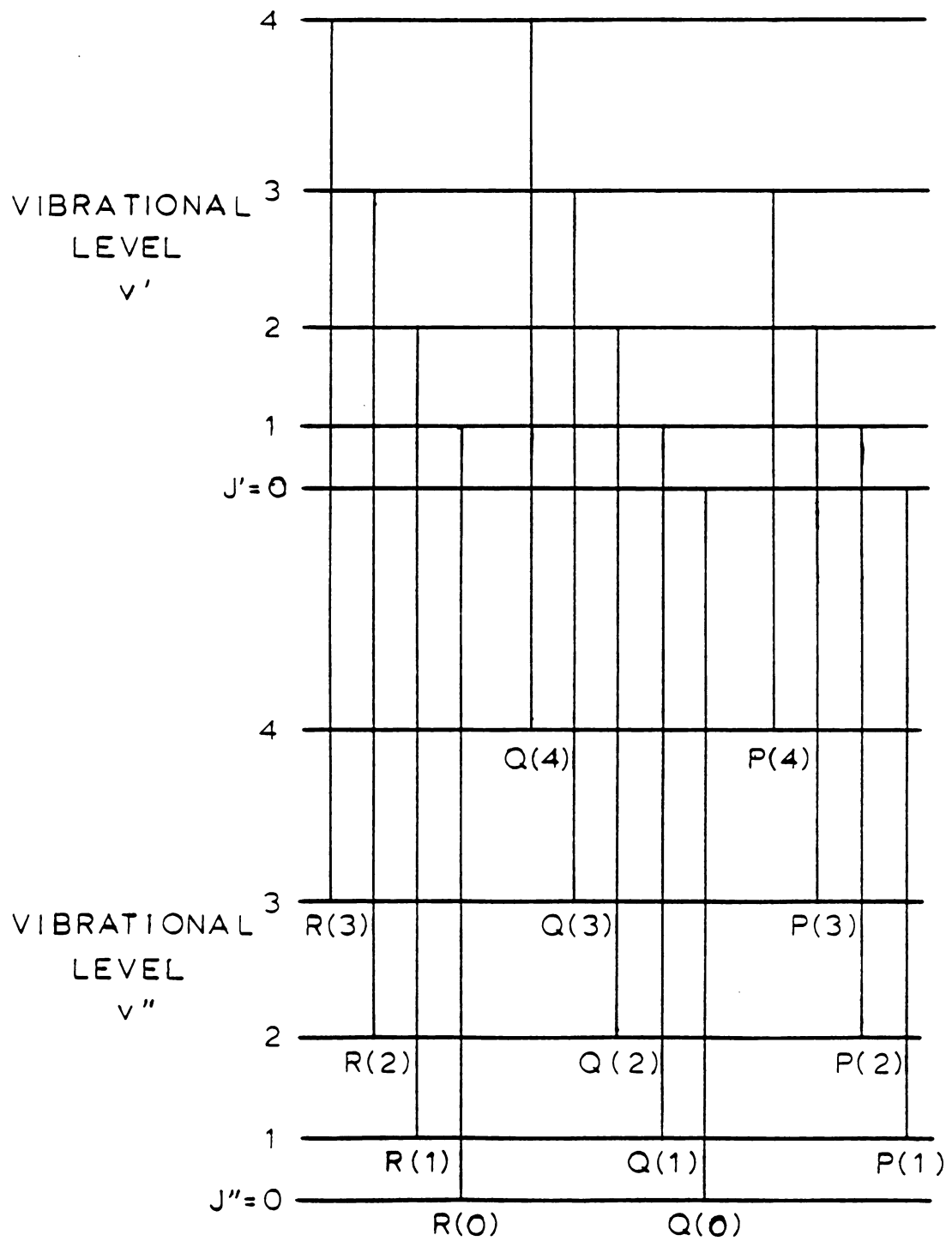

Figure 9. R, P, and Q branches of a rotational transition.

have a component along the internuclear axis, i.e., $\Lambda \neq 0$. However, the molecule is again viewed as rigid. Obviously, these models do not allow for molecular vibrations.

The nonrigid rotor model allows for the molecule to vibrate independently of the rotational motion. The vibrating rotor model allows for the rotational and vibrational motion to occur simultaneously. However, these two models do not allow for a component of the angular momentum along the internuclear axis.

The description of the interaction of the electronic and rotational motions is divided into different modes of coupling, known as Hund's coupling cases. The Hund's coupling cases distinguish the different ways in which the resultant total angular momentum, J, is formed. From the orientation possibilities of the vectors that form J, the corresponding quantum number can take on the value

$$J = +J, J-1, J-2, \cdots, -(J+1), -J$$

resulting in a 2J+1 - fold degeneracy for each rotational level.

A special case is the $^1\Sigma$ state, in which the electronic spin, S and orbital angular, $\mathbf{\Lambda}$, momentum are zero. The Hund's coupling cases are meaningless since that state possesses only nuclear rotational angular momentum, $\mathbf{N}$. J then takes on the values.

$$J = N = 1,2,3, \cdots$$

The rotational behavior is identically the rigid rotor. The two coupling cases that occur most frequently are Hund's case (a) and (b). There are other cases but they will not be discussed here.

In Hund's case (a), shown in Figure 10, it is assumed that the interaction of the electronic and nuclear rotational motions are very weak, with the electronic motion being strongly coupled to the internuclear axis. This case corresponds to the symmetric top model, and J characterizes the rotational levels.

$J = \Omega, \Omega+1, \Omega+2, \cdots$

The section rule for this case is $\Delta\Sigma = 0$; and if $\Omega = 0$ in both electronic states, $\Delta J = 0$ is forbidden.

In Hund's case (b), shown in Figure 11, the electronic spin singular momentum, S, is only weakly coupled to the internuclear axis. Ω is not defined for this case. The total angular momentum excluding spin is defined as K, and for this case, the corresponding quantum number, K, characterizes the rotational levels.

$K = \Omega, \Omega+1, \Omega+2, \cdots$

The values for J are then

$J = (K+S), (K+S-1), (K+S-2), \cdots, (K-S).$

Here the selection rule for a rotational transition becomes $\Delta K = 0, \pm 1$ with the restriction that $\Delta K = 0$ for a Σ-Σ transition is forbidden.

The symmetry properties of the rotational levels are determined by the behavior of the total eigenfunction (not the rotational eigenfunction alone) with respect to an inversion of all the particles (electrons and nuclei) about the origin. A positive, +, or negative, -, rotational level depends on whether the total eigenfunction remains unchanged or changes sign as a result of such an inversion, respectively. For the Σ state ($\Lambda = 0$) rotational levels are positive for K being even or odd and they are negative for K being odd or even. It can be shown that for Σ^+ states the even K-valued rotational levels are positive and the odd K-valued rotational levels

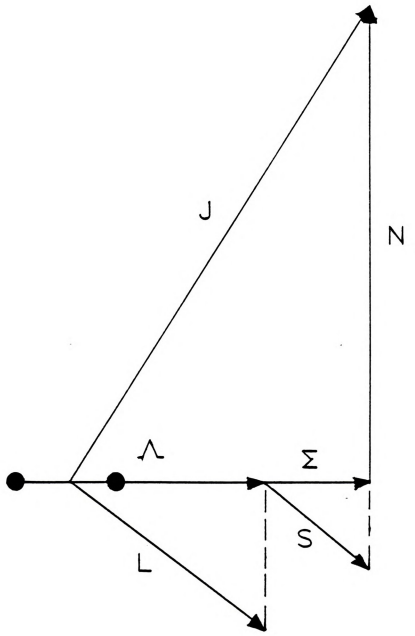

Figure 10. Diagram for Hund's case (a).

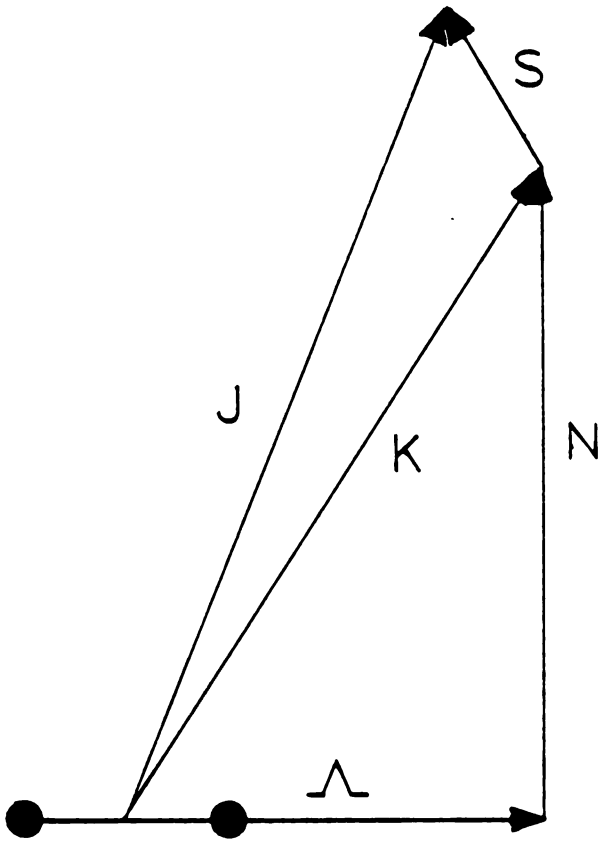

Figure 11. Diagram for Hund's case (b).

are negative, whereas for the Σ^- state, the opposite holds true. For the double degenerate states ($\Lambda > 0$; i.e., Π, Δ, $\cdots$), there is a positive and negative rotational level for each K value.

This degeneracy is removed with increasing rotation (J values), from the interaction of the rotation of the nuclei and the orbital angular momentum. This splitting is known as Λ-type doubling. This phenomena gives rise to two separate series, each of which behaves similar to a single Σ state with alternating positive/negative and symmetric/asymmetric rotational levels. The states that behave similar to a Σ^+ state are denoted, (+), (a) or (c); and those that behave similar to a Σ^- state are denoted (-), (b) or (d). In addition, in the case of the homonuclear diatomic molecule, it can be shown that the positive rotational levels are symmetric, (s), with the negative rotational levels being asymmetric,(a), for the even electronic states, g; and the negative levels are symmetric, (s), with the positive levels being asymmetric, (a), for the odd electronic states, u. The symmetries of the rotational levels of homonuclear diatomic molecules in the Σ states are shown in Figure 12. More selection rules for rotational transitions are that positive rotational levels can combine only with negative rotational levels

$$+ \leftrightarrow -$$

or $+ \not\leftrightarrow +$

$$- \not\leftrightarrow -$$

and, for molecules with indentical nuclei, that symmetric rotational levels can only combine with other symmetric rotational levels and likewise for the asymmetrical rotational levels.

$$s \leftrightarrow s$$

$$a \leftrightarrow a$$

or $s \not\leftrightarrow a$

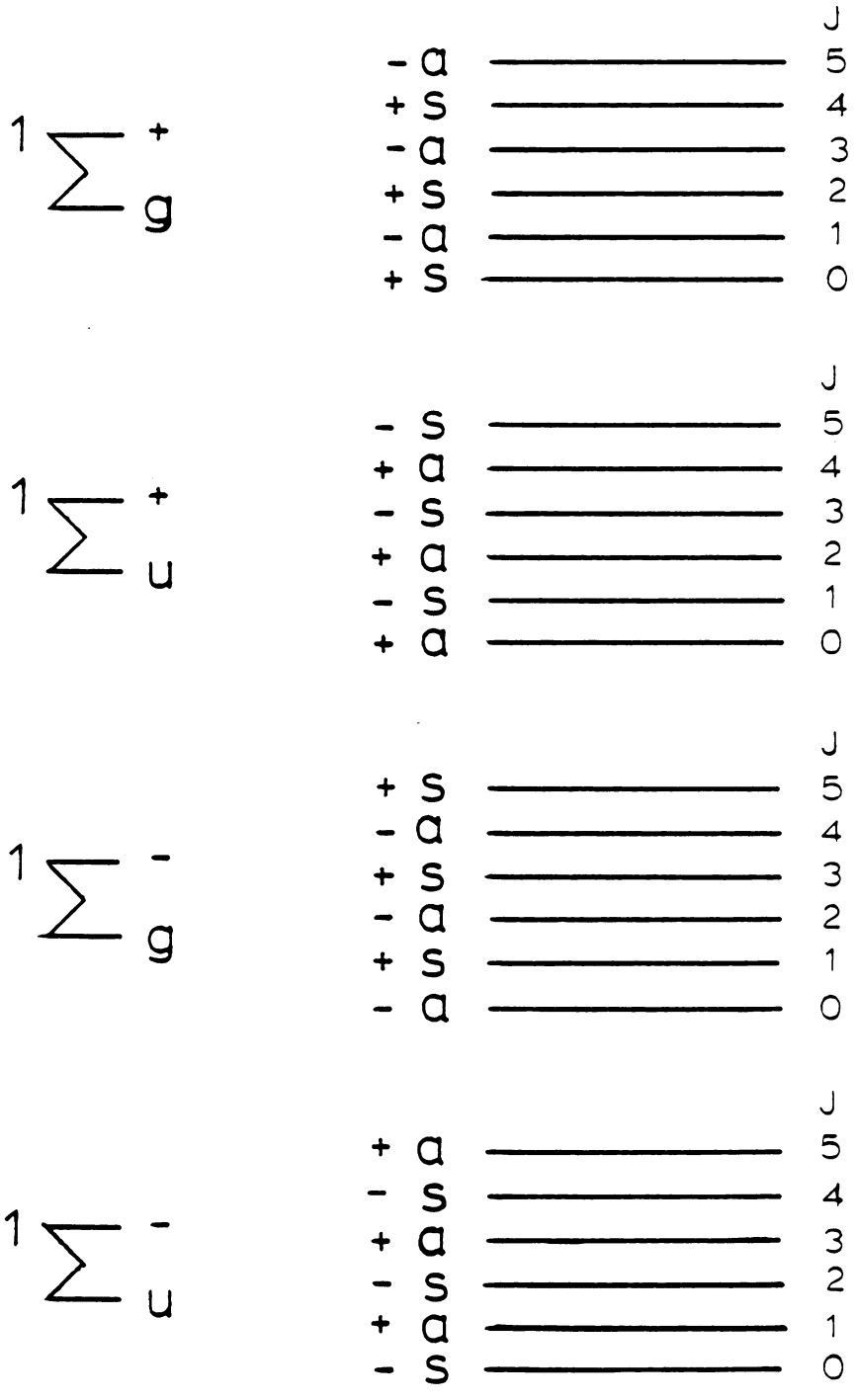

Figure 12. Rotational energy level symmetries of the Σ states.

Nuclear spin angular momentum has a great deal of influence on the symmetric and asymmetric rotational levels in a homonuclear molecule. The spin angular momentum, I, of the each nuclei form a resultant T, the total nuclear spin angular momentum of the diatomic molecule. The nuclear spin state is characterized by the quantum number T, where T = 2I, 2I-1, ···, 0. A state with a given value of T has a statistical weight of 2T+1. It can be shown that the even values of T accompany the symmetric levels and the odd values of T accompany the asymmetric levels. In the case of integral T, nuclei which follow Bose statistics, the statistical weight of the symmetrical and asymmetrical levels is (2I+1)(I+1) and (2I+1)I, respectively. In the case of half-integral I, nuclei which follow Fermi statistics, the opposite is true. In either case, the ratio, R, of the strong to weak rotational level is

$$R = \frac{I + 1}{I}$$

The spectra obtained from homonuclear molecules has alternating strong and weak rotational lines, and the magnitude of these alternating intensities depends on the nuclear spin of the atoms in the molecule. The oxygen atom has zero nuclear spin resulting in the spectra of having every other rotational line missing. The deuterium and nitrogen atoms have nuclear spins of 1, resulting in alternating intensities of 2 to 1. The hydrogen atom has a nuclear spin of 1/2, resulting in an alternation of 3 to 1 for the molecular hydrogen spectra. For the hydrogen case, the asymmetric levels have a statistical weight of 3 and the symmetric levels have a statistical weight of 1. Since the nuclear spins in the hydrogen molecule are orientated either parallel or antiparallel, and since the symmetric and asym-

metric levels do not interact; the gas can be considered to be a mixture of two modifications, designated as ortho- and para-hydrogen, respectively.

Theory shows that the ground state of the hydrogen molecule is $1s^1\Sigma_g^+$. Utilizing the appropriate selection rules, the Lyman band transitions can be identified and are shown in Figure 13. Likewise, the $3d^1\Sigma \rightarrow 2p^1\Sigma$ and $3d^1\Pi \rightarrow 2p^1\Sigma$ transitions, that radiate in the visible region, can be identified and are shown in Figures 14 and 15, respectively. The vibrational levels v' and v" involved in these electronic transitions are arbitrary, also only the first few rotational levels are shown. In the determination of these transitions, the distinction between the Hund's coupling cases is meaningless since these electronic states posess zero spin. The transition probability matrix element, $|R^{nm}|^2$, describes the intensity for an individual rotational transition. This matrix element is the overlap integral of the electric dipole and the wave functions of the two energy states, n and m. The matrix element for the rotational lines of a vibrational band in an electronic transition, can be separated into two parts. One involves the vibrational and electronic wave functions which will be constant for all the rotational lines. The other involves only the rotational wave functions. That part of the matrix element which only involves the rotational wave function is designated the line strength, S_J.

The matrix element for all the rotational lines in a single vibrational band of an individual electronic transition is then

$$|R^{nm}|^2 = \text{const} \cdot S_J^{nm}$$

The intensity of a single rotational line of the spontaneous radiation emitted by an eletric dipole can then be expressed as

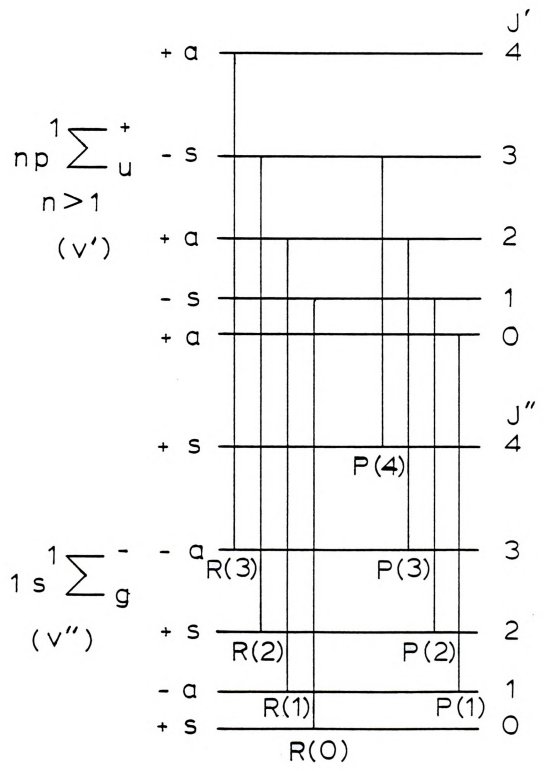

Figure 13. Rotational lines of the $np\,^1\Sigma_u^+ \rightarrow 1s\,^1\Sigma_g^+$ transitions.

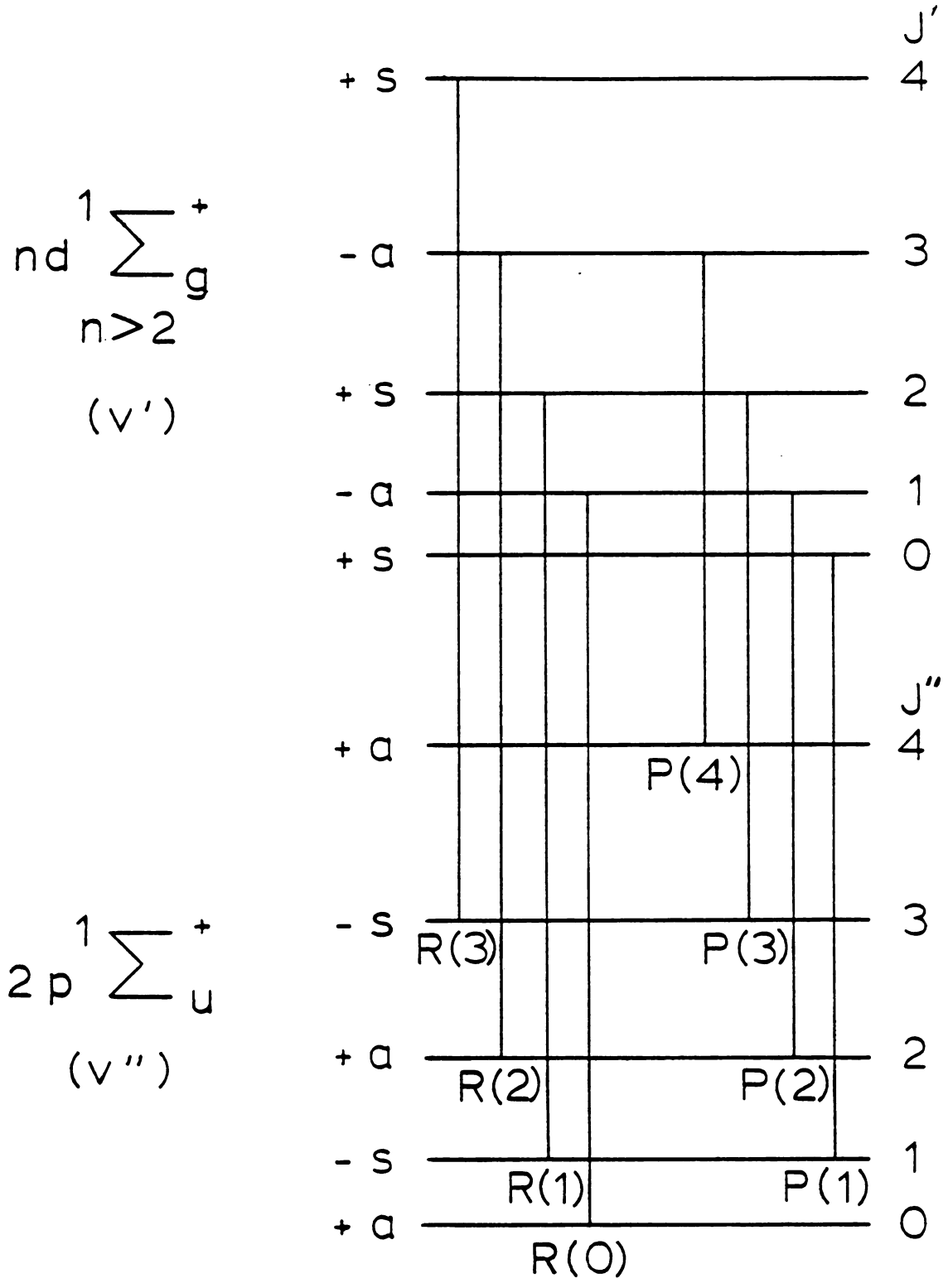

Figure 14. Rotational lines of the $nd\,^1\Sigma_g^+ \rightarrow 2p\,^1\Sigma_u^+$ transitions.

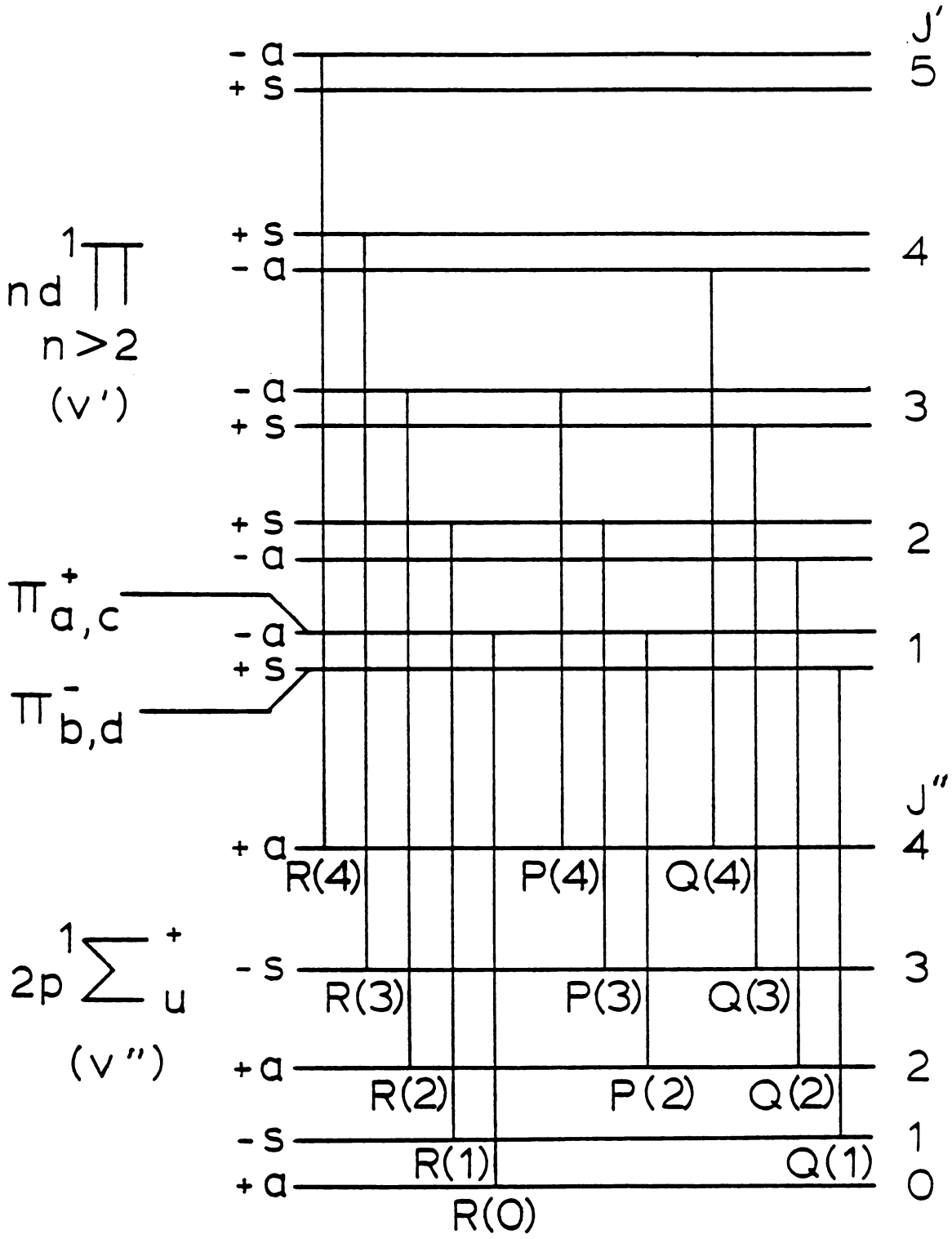

Figure 15. Rotational lines of the $nd'\Pi \rightarrow 2p'\Sigma^+_u$ transitions.

$$I_{em}^{nm} = \frac{C_{em}\,\nu_{nm}^{4}\,S_J^{nm}}{Q_{rot}}\, e^{-E_n/kT_{rot}}$$

where C_{em} is a constant, and n and m now denote rotational levels in the particular vibrational states of the electronic states involved. The rotational temperature, T_{rot}, characterizes the thermal distribution of the rotational levels in the initial vibrational and electronic states. The rotational partition function, Q_{rot}, is summed over all the rotational levels of the initial energy state involved in the transition and is a constant. Expressions for the theoretical line strengths for the symmetric top rotational model have been determined.

For $\Delta\Lambda = 0$

$$S_J^R = \frac{(J'' + 1 + \Lambda'')(J'' + 1 - \Lambda'')}{J'' + 1} = \frac{(J' + \Lambda')(J' - \Lambda')}{J'}$$

$$S_J^Q = \frac{(2J'' + 1)\,\Lambda''^2}{J''\,(J'' + 1)} = \frac{(2J' + 1)\,\Lambda'^2}{J'\,(J' + 1)}$$

$$S_J^P = \frac{(J'' + \Lambda'')(J'' - \Lambda'')}{J''} = \frac{(J' + 1 + \Lambda')(J' + 1 - \Lambda')}{J' + 1}$$

For $\Delta\Lambda = +1$

$$S_J^R = \frac{(J'' + 2 + \Lambda'')(J'' + 1 + \Lambda'')}{4\,(J'' + 1)} = \frac{(J' + \Lambda')(J' - 1 + \Lambda')}{4\,J'}$$

$$S_J^Q = \frac{(J'' + 1 + \Lambda'')(J'' - \Lambda'')(2J'' + 1)}{4\,J''\,(J'' + 1)}$$

$$= \frac{(J' + \Lambda)(J' + 1 - \Lambda)(2J' + 1)}{4\,J'\,(J' + 1)}$$

$$S_J^P = \frac{(J'' - 1 - \Lambda'')(J'' - \Lambda'')}{4\,J''} = \frac{(J' + 1 - \Lambda')(J' + 2 - \Lambda')}{4\,(J' + 1)}$$

For $\Delta\Lambda = -1$

$$S_J^R = \frac{(J'' + 2 - \Lambda'')(J'' + 1 - \Lambda'')}{4\,(J'' + 1)} = \frac{(J' - \Lambda')(J' - 1 - \Lambda')}{4\,J'}$$

$$S_J^Q = \frac{(J'' + 1 - \Lambda'')(J'' + \Lambda'')(2J'' + 1)}{4\ J''\ (J'' + 1)}$$

$$= \frac{(J' - \Lambda')(J' + 1 + \Lambda')(2J' + 1)}{4\ J'\ (J' + 1)}$$

$$S_J^P = \frac{(J'' - 1 + \Lambda'')(J'' + \Lambda'')}{4\ J''} = \frac{(J' + 1 + \Lambda')(J' + 2 + \Lambda')}{4\ (J' + 1)}$$

For the transition $\Lambda' = 0 \rightarrow \Lambda'' = 0$, these expressions reduce to those for the rigid rotor rotational model.

$$S_J^R = J'' + 1 = J'$$

$$S_J^P = J'' = J' + 1$$

These formulas are exact and are independent of any thermal equilibrium assumption. The line strengths are also the statistical weights. The sum of the line strengths (S_J^R, S_J^P, and S_J^Q when applicable) for a particular value of J' or J" yields the degeneracy (statistical weight), 2J'+1 or 2J"+1, of that rotational level J' or J", respectively.

If the frequency range over which the spectra is taken is sufficiently small, which is usually the case, the ν_{nm}^4 dependence in the intensity equation may be regarded as constant. The energy, E_n, of the rotational levels may be expressed as rotational terms, F(J), with units of cm^{-1}

$$E_n = F(J)hc$$

The intensity of a single rotational line is now given as

$$I_{em}^{nm} = C'_{em}\ S_J^{nm}\ e^{-F(J)hc/kT_{rot}}$$

$$\text{where } C'_{em} = \frac{C_{em}\ \nu_{nm}^4}{Q_{rot}}$$

The intensity of the electromagnetic radiation that is actually measured by the spectrometer is given by

$$I_{meas} = I_{em}^{nm} \frac{R_\lambda \, d\Omega}{4\pi}$$

where R_λ is the instrumental response function and $\frac{d\Omega}{4\pi}$ is the normalized solid angle of the spectrometer.

Again, if the frequency range is sufficiently small, R_λ will be a constant. The solid angle is also a constant under normal operating conditions. The intensity measured for a single rotational line, dropping the n's and m's, becomes

$$I_{meas} = C \, S_J \, e^{-F(J)hc/kT_{rot}}$$

$$\text{where } C = \frac{C'_{em} \, R_\lambda \, d\Omega}{4\pi}$$

Taking the natural log of this expression

$$\ln\left(\frac{I_{meas}}{S_J}\right) = \ln C - \frac{F(J)hc}{kT_{rot}}$$

II. Calculations and Results

Emission spectra were taken of the discharge between 3000-5000 Å. The strongest rotational branch of nine vibrational bands of two electronic transitions were identified, and are given in Table 1.

The four transitions in Table 1 denoted by *, were found to be the strongest bands which could be completely resolved. Rotational temperatures were determined from these four bands yielding four independent measurements of the rotational temperature for each experimental condition.

TABLE 1

TRANSITIONS IDENTIFIED

Electronic Transition	Vibrational Transition	Strongest Rotational Branch
$3d^1\Sigma_g^+ \rightarrow 2p^1\Sigma_u^+$	0 - 0 *	R
	1 - 0 *	R
	2 - 1	R
	0 - 1	R
$3d^1\Pi_b \rightarrow 2p^1\Sigma_u^+$	0 - 0 *	Q
	1 - 0 *	Q
	2 - 1	Q
$3d^1\Pi_a \rightarrow 2p^1\Sigma_u^+$	0 - 0	P
	1 - 0	P

The wavelengths of the rotational lines that were observed and analyzed for the four transitions are given in Table 2 (Richardson, 1934). The energies of the initial states of these transitions are given in Table 3 (Dieke, 1958).

For each experimental condition, the spectra of the transitions were taken and the intensities of the rotational lines were obtained. The height of the peaks was measured as opposed to integrating the line profile since the wavelength range involved was small and the half widths for the lines were approximately constant.

A semilogarithmic plot of I_{meas}/S_J as a function of energy, F(J), gives a straight line with a slope of $-hc/kT_{rot}$ and an intercept of ln C. A best "fit" for the straight line

$$y = m\,x + b$$

where $x = F(J)$

$$y = \ln\left(\frac{I_{meas}}{S_J}\right)$$

was obtained from the data, utilizing the theory of linear least squares and taking into account the alternating intensities of 3 and 1 for ortho- and para-hydrogen respectively. The slope, m; the intercept, b; and their uncertainties, Δm and Δb; were calculated from the data (Meyer, 1975)

$$m = \frac{\left(\sum\frac{1}{\Delta y^2}\right)\left(\sum\frac{xy}{\Delta y^2}\right) - \left(\sum\frac{x}{\Delta y^2}\right)\left(\sum\frac{y}{\Delta y^2}\right)}{DET}$$

$$b = \frac{\left(\sum\frac{x^2}{\Delta y^2}\right)\left(\sum\frac{y}{\Delta y^2}\right) - \left(\sum\frac{xy}{\Delta y^2}\right)\left(\sum\frac{x}{\Delta y^2}\right)}{DET}$$

$$(\Delta m)^2 = \frac{\left(\sum\frac{1}{\Delta y^2}\right)}{DET}$$

TABLE 2

WAVELENGTHS OF THE ROTATIONAL LINES

$3d^1\Sigma_g^+ \rightarrow 2p^1\Sigma_u^+$

Transition 1 (0 - 0)		Transition 2 (1 - 0)	
R	Wavelength (Å)	R	Wavelength (Å)
0	4627.98	0	4195.67
1	4631.45	1	4199.78
2	4634.03	2	4205.10
3	4634.59	3	4210.13
4	4631.85	4	4212.50
5	4625.31	5	4212.03
6	4618.30	6	4209.17
		7	4202.43
		8	4189.45

$3d^1\Pi_b \rightarrow 2p^1\Sigma_u^+$

Transition 3 (0 - 0)		Transition 4 (1 - 0)	
Q	Wavelength (Å)	Q	Wavelength (Å)
1	4579.45	1	4177.72
2	4579.99	2	4177.12
3	4578.01	3	4175.16
4	4572.71	4	4171.29
5	4563.72	5	4165.19
6	4550.98	6	4156.62
7	4534.46	7	4145.55
8	4514.31	8	4131.98

TABLE 3

ENERGIES OF THE MOLECULAR STATES

$3d^1\Sigma_g^+$		
J	v = 0	v = 1
0	0	0
1	-7.52	-13.80
2	15.15	1.70
3	80.44	48.92
4	192.86	135.59
5	357.38	273.92
6	574.86	463.48
7	828.36	700.35
8	879.55	---

$3d^1\Pi_b$		
J	v = 0	v = 1
1	0	0
2	74.70	80.73
3	199.18	206.98
4	376.21	380.83
5	606.19	602.96
6	888.30	873.16
7	1220.66	1189.65
8	1601.27	1551.21

$$(\Delta b)^2 = \frac{\left(\sum \frac{x^2}{\Delta y^2}\right)}{DET}$$

where

$$DET = \left(\sum \frac{1}{\Delta y^2}\right)\left(\sum \frac{x^2}{\Delta y^2}\right) - \left(\sum \frac{x}{\Delta y^2}\right)^2$$

$$\Delta y^2 = \left(\frac{I_{meas}}{\Delta I_{meas}}\right)^2$$

How well the data is represented by the straight line obtained from the linear least squares technique can be evaluated with two values; χ^2 and the correlation coefficient, r.

$$\chi^2 = \sum \frac{(y - mx - b)^2}{\Delta y^2}$$

$$r = \frac{\left(\sum \frac{1}{\Delta y^2}\right)\left(\sum \frac{xy}{\Delta y^2}\right) - \left(\sum \frac{x}{\Delta y^2}\right)\left(\sum \frac{y}{\Delta y^2}\right)}{\left[\left(\sum \frac{1}{\Delta y^2}\right)\left(\sum \frac{x^2}{\Delta y^2}\right) - \left(\sum \frac{x}{\Delta y^2}\right)^2\right]^{\frac{1}{2}}\left[\left(\sum \frac{1}{\Delta y^2}\right)\left(\sum \frac{y^2}{\Delta y^2}\right) - \left(\sum \frac{y}{\Delta y^2}\right)^2\right]^{\frac{1}{2}}}$$

A perfect "fit" results in the values $\chi^2 = 0$ and $|r| = 1$. The worse the fit is, the larger χ^2 and smaller $|r|$ become. The summations in these equations are over all the rotational lines of a transition that were measured.

The rotational temperature and its uncertainty were then calculated from the slope and its uncertainty.

$$T_{rot} = \frac{-hc}{mk}$$

and

$$\Delta T_{rot} = \frac{k\, T_{rot}^2}{h\, c}\, \Delta m$$

It should be noted that the intercept is not used in the calculation of the rotational temperature and that the instrumental and geometrical variables of the intensity measurements show up only in the intercept.

The rotational temperatures and their uncertainties are given in Table 4. Figures 16 thru 19 show the rotational temperatures obtained from the various transitions as a function of absorbed power, for a given flow rate (pressure). Figure 20 shows the rotational temperatures averaged over all the transitions as a function of absorbed power, for the various flow rates (pressures).

As can be seen from these figures, the rotational temperature generally increases with increasing flow rate (pressure) and absorbed power. The temperatures calculated from the various transitions are consistently different. The Q branches of transitions 3 and 4 yield the highest temperatures, the R branch of transition 2 yields the next highest temperature and the R branch of transition 1 yields the lowest temperature. These differences are larger than the experimental error at the lower flow rates (pressures) and become negligible at the higher flow rates (pressures). This observation would tend to suggest that thermal equilibrium is achieved at the higher pressures but not at the lower ones.

The dominant factor in the uncertainty of the temperature estimate is the error involved in the emission line intensity measurement. The uncertainty for the intensity measurements results from two major sources, the photomultiplier tube and the microwave power source. The emission intensity decreases with increasing pressure resulting in an increasing experimental error with increasing pressure. The inherent noise of the system does increase somewhat

TABLE 4

ROTATIONAL TEMPERATURE DATA

Flow Rate = 13.1 sccm

Power Absorbed	Transition 1	2	3	4	Average
280	566 ± 6	602 ± 14	641 ± 14	638 ± 12	612 ± 10
340	604 ± 4	631 ± 19	678 ± 9	664 ± 11	644 ± 11
404	616 ± 8	677 ± 17	710 ± 10	663 ± 12	667 ± 12
460	653 ± 9	666 ± 35	722 ± 23	750 ± 23	697 ± 23
536	679 ± 10	——	——	——	——
614	713 ± 15	——	——	——	——
676	737 ± 23	859 ± 42	885 ± 24	887 ± 22	807 ± 26

Flow Rate = 86.8 sccm

Power Absorbed	Transition 1	2	3	4	Average
276	610 ± 17	672 ± 42	734 ± 37	635 ± 18	645 ± 25
344	656 ± 15	670 ± 32	754 ± 25	678 ± 20	690 ± 25
400	678 ± 14	720 ± 28	815 ± 20	723 ± 22	723 ± 19
460	705 1± 14	——	——	——	——
534	727 ± 22	——	——	——	——
614	779 ± 23	——	——	——	——
680	834 ± 27	993 ± 69	1017 ± 34	939 ± 34	909 ± 36

TABLE 4
(Continued)

Flow Rate = 261.6 sccm

Power Absorbed	Transition 1	2	4	Average
282	662 ± 47	627 ± 108	726 ± 56	676 ± 60
340	718 ± 44	750 ± 108	727 ± 47	726 ± 57
400	759 ± 48	——	728 ± 52	782 ± 57
460	791 ± 53	——	——	——
524	830 ± 56	——	——	——
618	865 ± 55	——	——	——
684	886 ± 47	1033 ± 107	1010 ± 63	940 ± 62

Flow Rate = 544.6 sccm

Power Absorbed	Transition 1	2	4	Average
290	768 ± 99	692 ± 185	881 ± 72	755 ± 130
342	754 ± 120	691 ± 188	786 ± 147	——
400	831 ± 113	858 ± 246	825 ± 121	835 ± 139
464	841 ± 100	——	——	——
620	898 ± 126	——	——	——
696	923 ± 97	1064 ± 273	1061 ± 135	979 ± 140

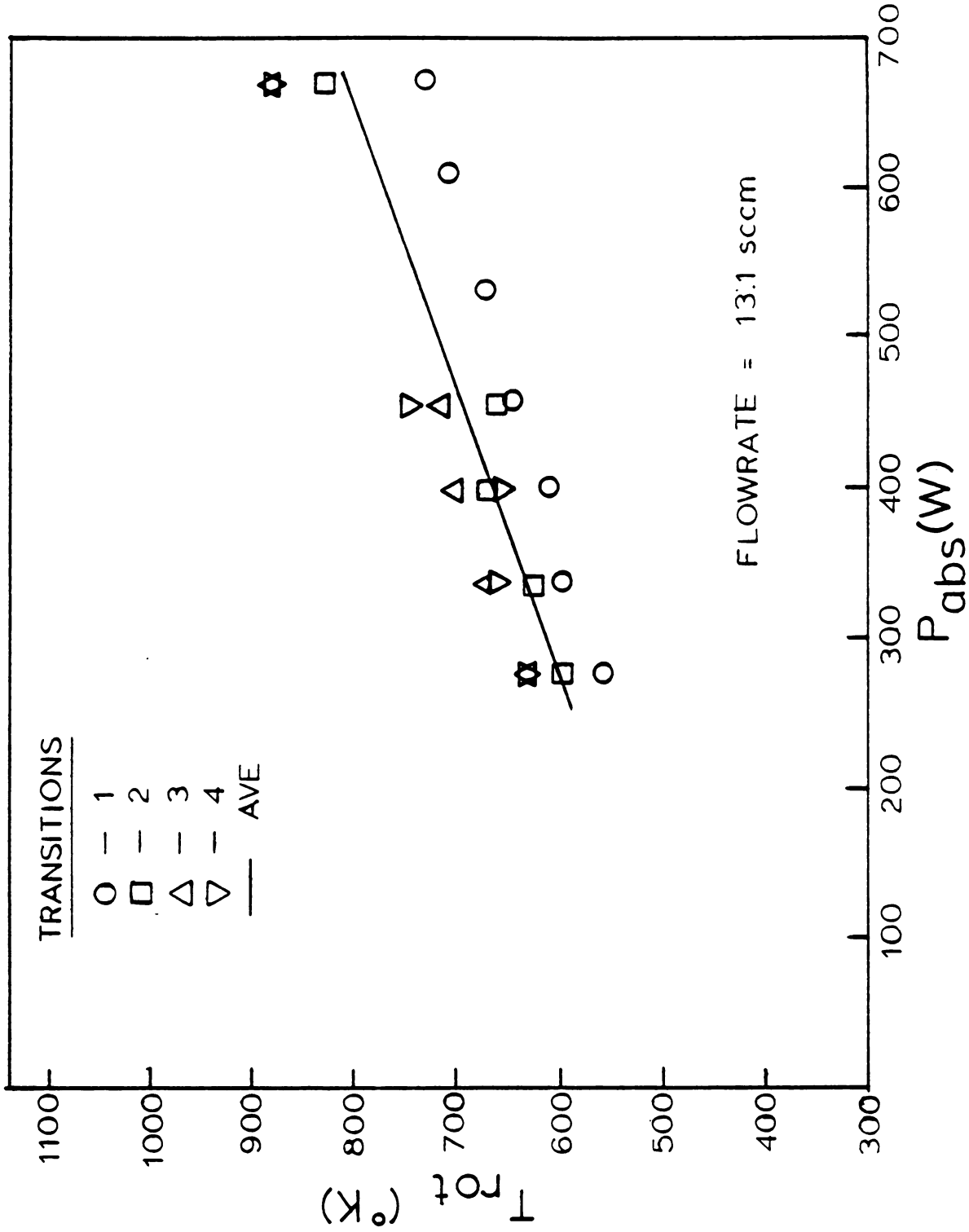

Figure 16. Rotational temperatures as functions of absorbed power at 13.1 sccm.

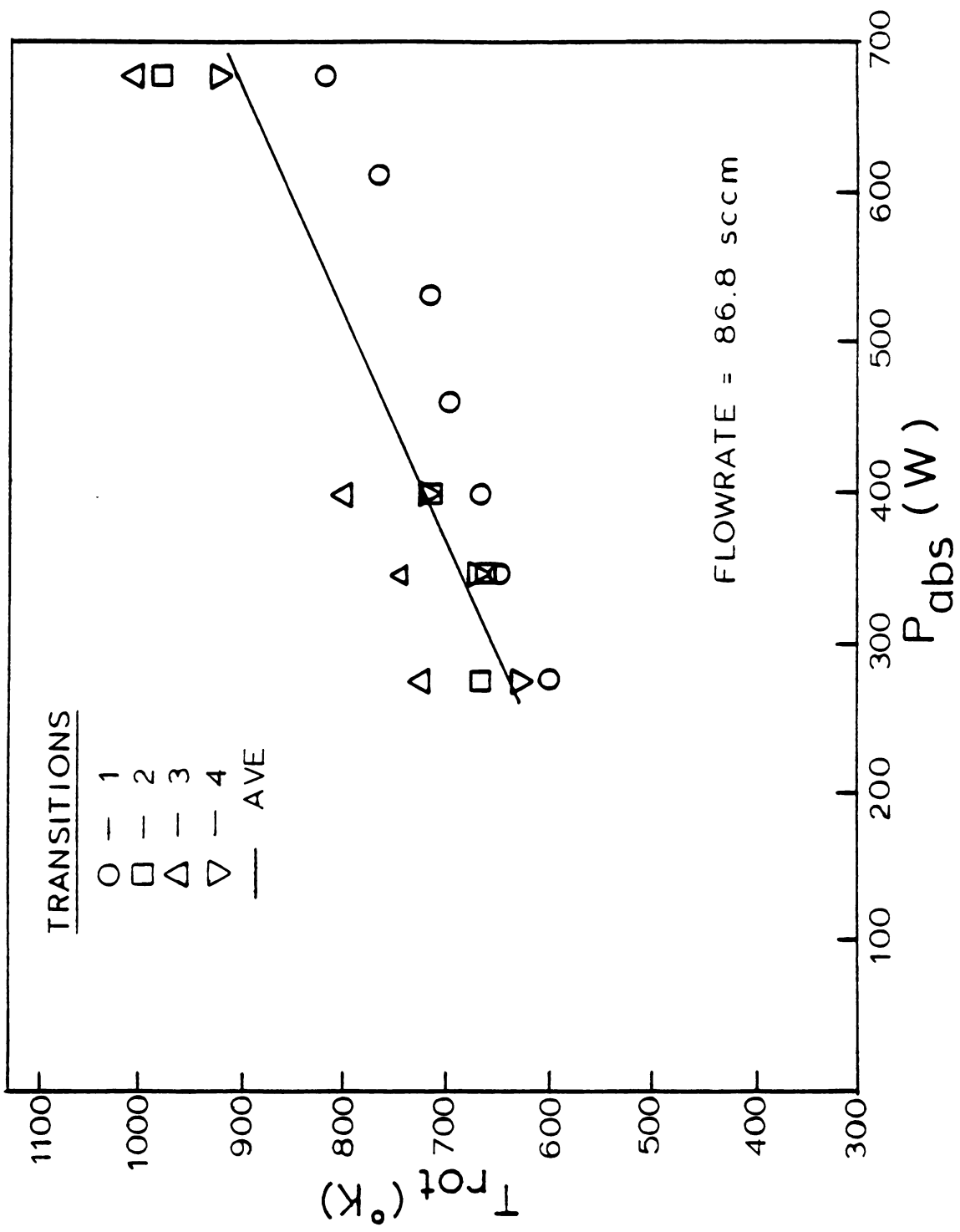

Figure 17. Rotational temperatures as functions of absorbed power at 86.8 sccm.

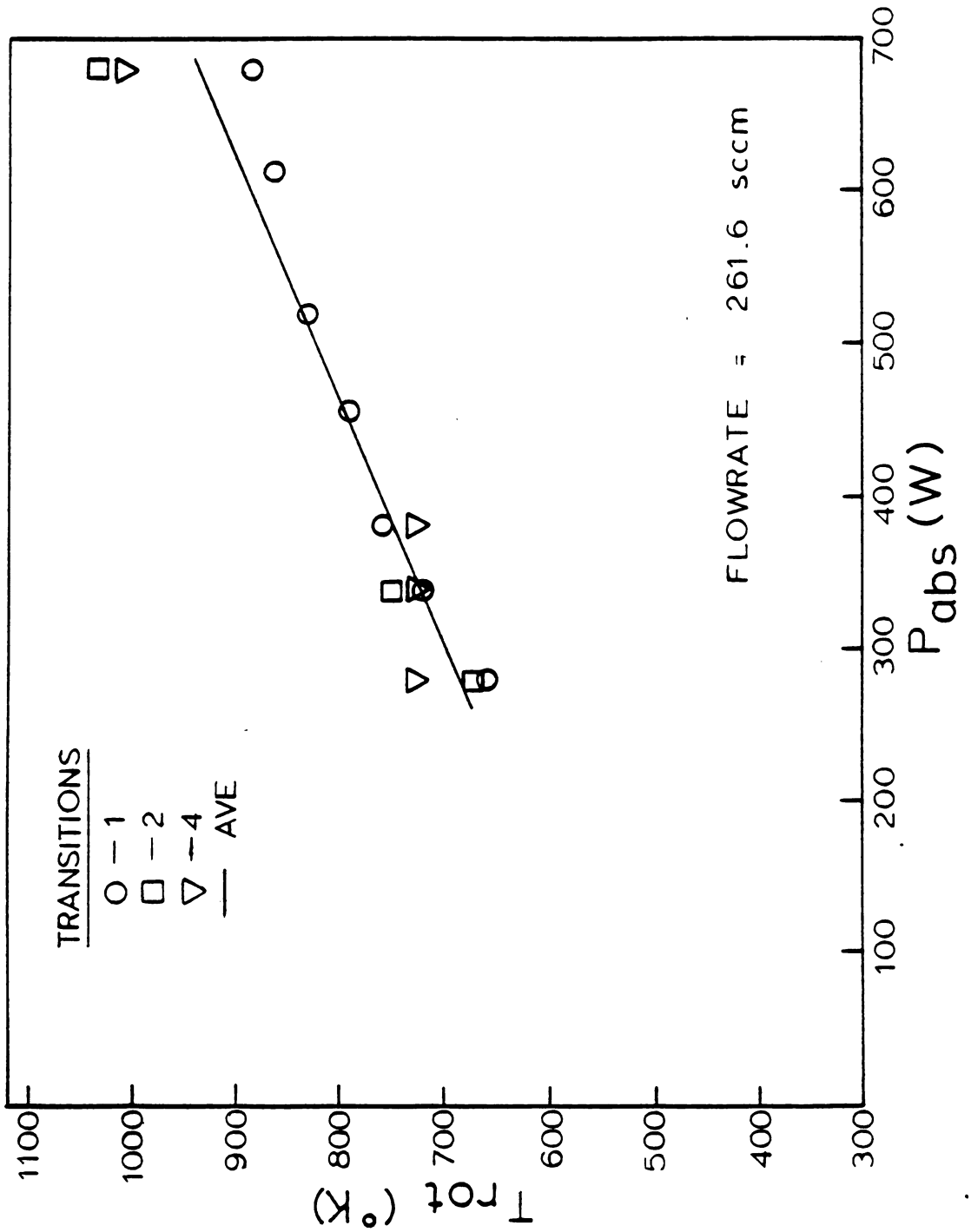

Figure 18. Rotational temperatures as functions of absorbed power at 261.6 sccm.

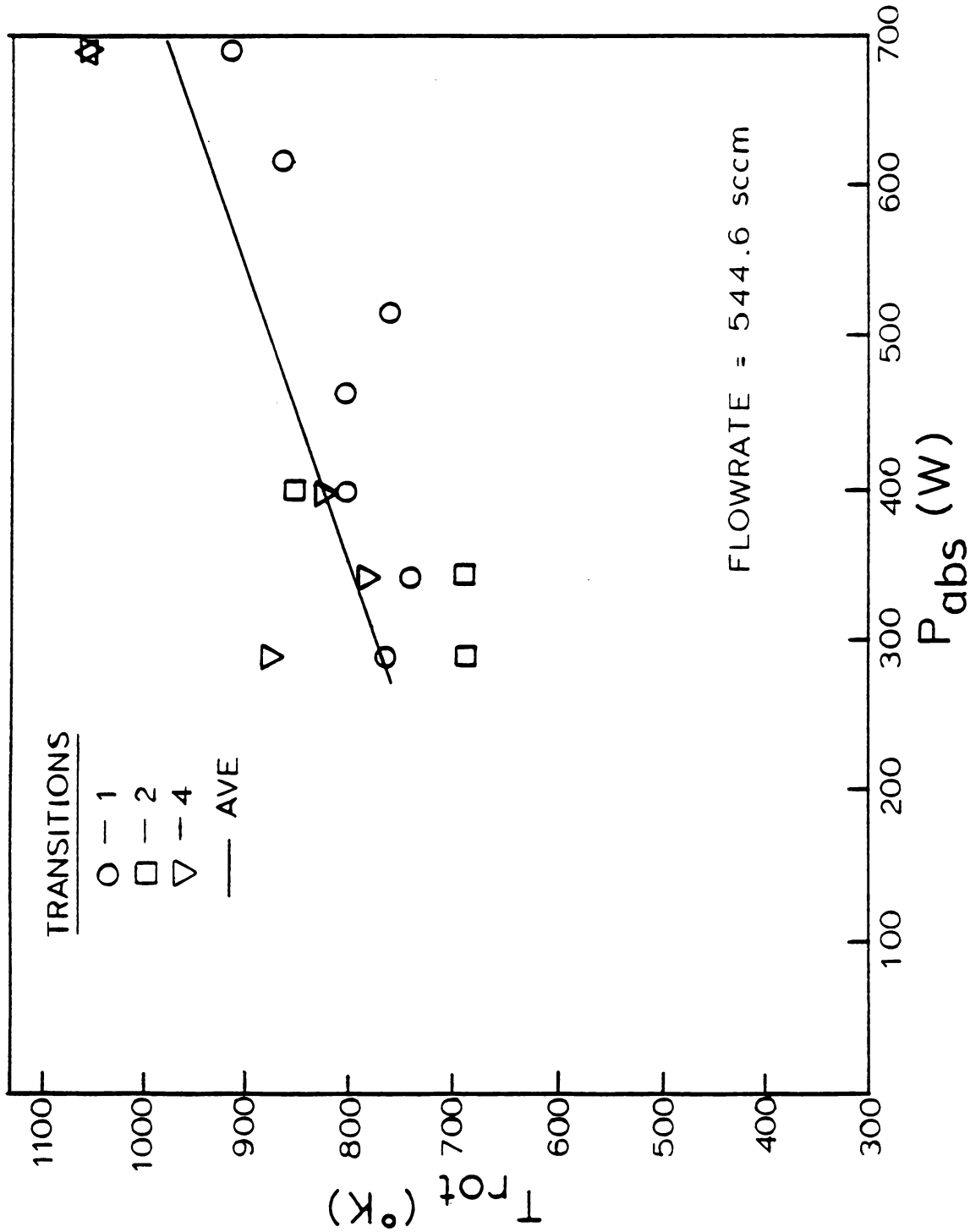

Figure 19. Rotational temperatures as functions of absorbed power at 544.6 sccm.

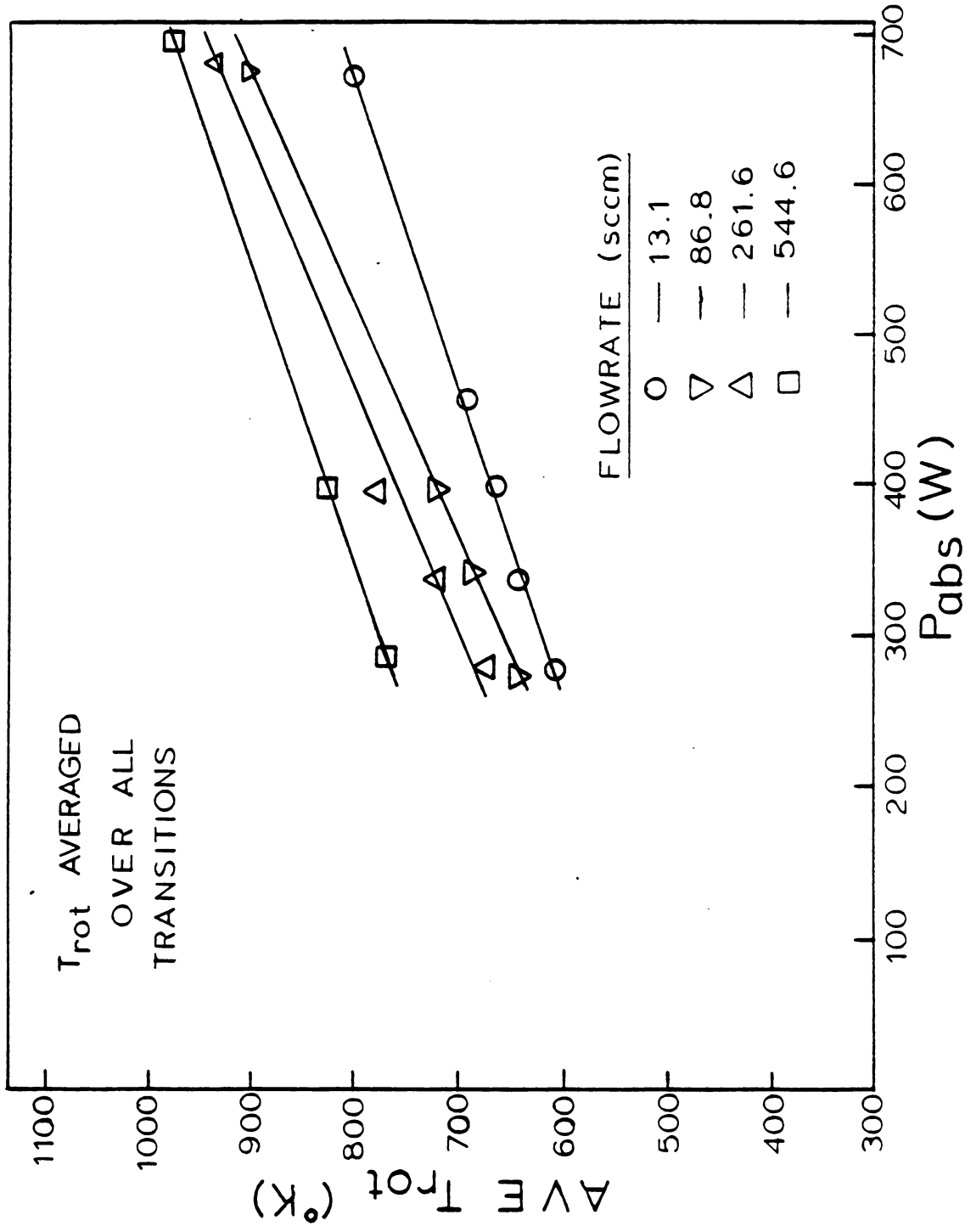

Figure 20. Average rotational temperature as a function of absorbed power for various flowrates.

with increasing absorbed power levels, but it is negligible compared to the effect of the decreasing intensity with increasing pressure. The rotational lines of transition 1 are the most intense molecular lines, with the lines of other transitions being somewhat weaker.

The "goodness" of the linear least squares fit of the data also contributes to the uncertainty in the temperature results. The Q branches of transitions 3 and 4 give the best "fit" in terms of χ^2 and the correlation coefficient, r. The R branch of transition 1 gives the next best correlation coefficient and the worst χ^2 value. The R branch of transition 2 gives the worst correlation coefficient and the second best χ^2 value.

The combination of all the factors result with the R branch of transition 1 having the smallest temperature uncertainties, the Q branches of transitions 3 and 4 having the next smallest temperature uncertainties, and the R branch of transition 2 having the largest temperature uncertainty. The temperatures calculated seem to be a somewhat linear function of the absorbed power for this range of experimental conditions, expecially when the uncertainty of the temperature is taken into consideration. However, that straight line does not go to room temperature as the absorbed power goes to zero.

The reproducibility of the temperature measurements is very good. For a given transition and a given experimental condition, the temperature measurements agree to within the experimental error at the lower pressures (flow rates) and to within 50% of the experimental error at the higher pressures (flow rates). At the lower pressures (flow rates), it is difficult to determine which transition gives the most accurate temperatures. At the higher pressures (flow rates), the R branch of transition 1 must be considered to give the most accurate

temperatures, since that temperature estimate possesses the smallest error. However, this result is due to the experimental set up and not to the theory involved or the molecular dynamics.

GAS DYNAMIC TEMPERATURE

I. Theoretical Background

A nozzle is a device that interchanges the enthalpy and the kinetic energy of a working fluid as a result of changing the cross-sectional area available for flow (Shapiro, 1953). In the study of the flow of compressible fluids through nozzles, the speed of sound is of major importance. The speed of sound, c, in a medium is the velocity at which an infinitesimal pressure perturbation propagates through that stationary medium, i.e., a sound wave.

Consider a wave front moving with velocity c through a stationary fluid as in Figure 21. The fluid to the right of the wave front has enthalpy H, pressure P, density ρ, and zero velocity. The fluid to the left of the wave front, through which the wave has already passed, has enthalpy H + dH, pressure P + dP, density ρ + dρ, and velocity du.

Now consider the same situation with the frame of reference moving along the wavefront as in Figure 22. An energy balance for this system can be written as

$$(H + dH) + 1/2\ (c - du)^2 = H + 1/2\ c^2 \qquad (1)$$

Since the sound wave is considered to be an infinitesimal pressure perturbation, it can be assumed to be reversible. In addition, since sound waves possess such high velocities, it can be assumed that there is negligible heat transfer and therefore adiabatic. Finally, since the process is both adiabatic and reversible, it is also isentropic.

Neglecting second order differentials, the energy balance becomes

$$dH = c\,du \qquad (2)$$

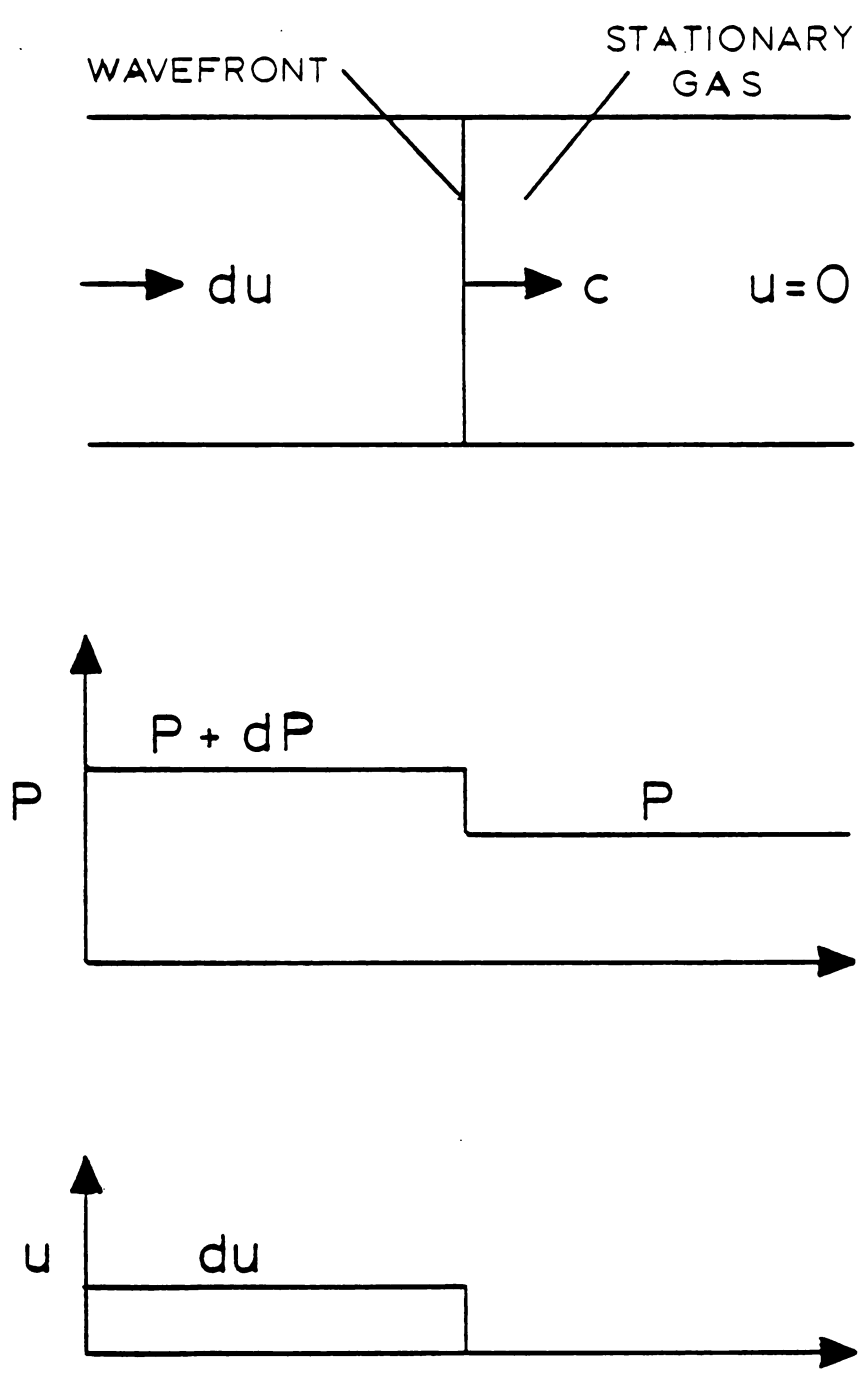

Figure 21. Wavefront moving through a stationary fluid with velocity c.

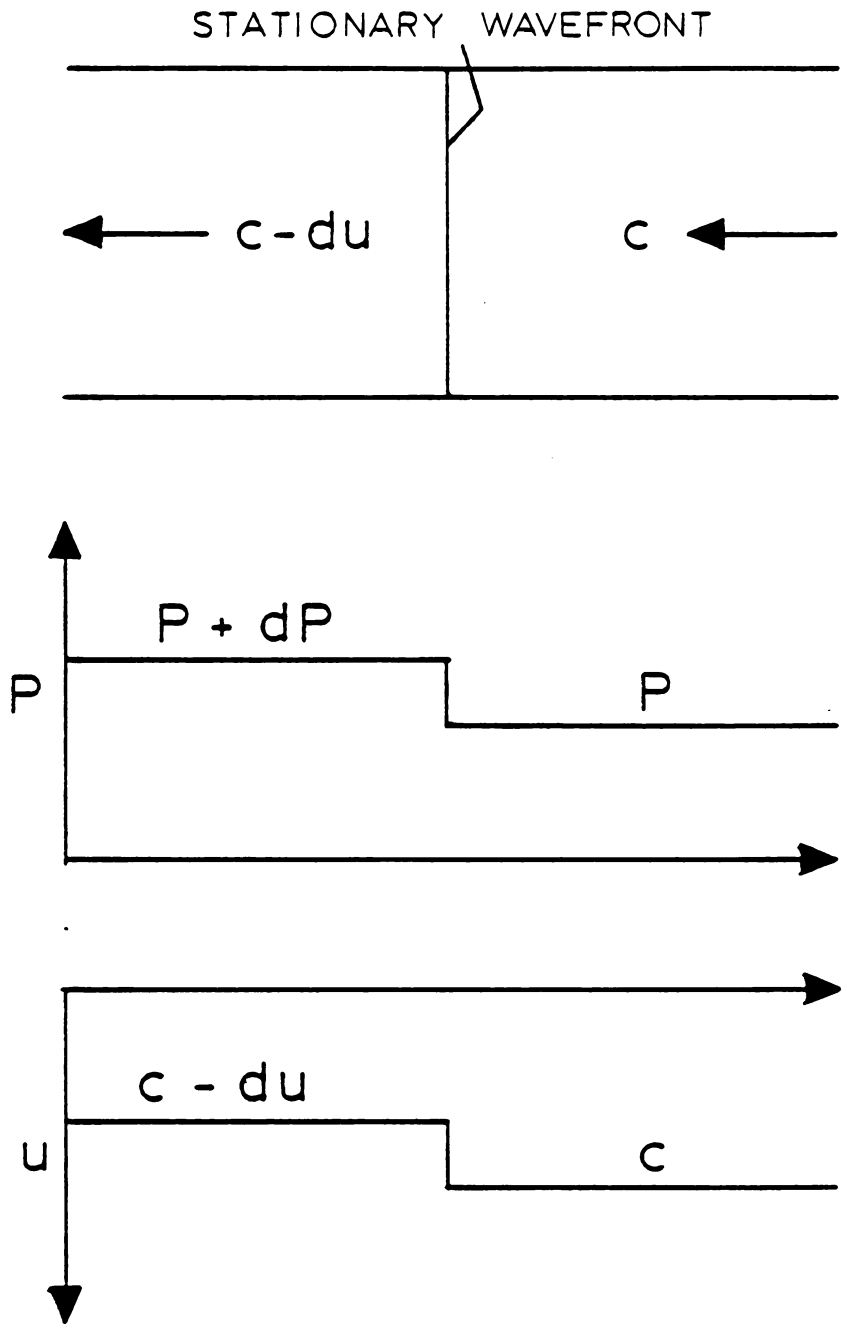

Figure 22. Wavefront moving with velocity c through a stationary fluid viewed with respect to the wavefront.

From thermodynamics

$$U = Q - W \tag{3}$$

$$H = U + PV \tag{4}$$

So

$$H = Q - W + PV$$

Taking the derivative

$$dH = dQ - dW + PdV + VdP \tag{5}$$

From the definitions of work and entropy

$$dW_{rev} = PdV \tag{6}$$

$$dQ_{rev} = TdS \tag{7}$$

Substituting for dW and dQ in eq. 5

$$dH = TdS + VdP$$

Equating eqs. 2 and 8

$$TdS + VdP = c\,du$$

Assuming $dS = 0$

$$VdP = c\,du$$

Since

$$V = \frac{1}{\rho}.$$

Then

$$\frac{1}{\rho}\,dP = c\,du \tag{8}$$

A mass balance on the system can be written as

$$(\rho + d\rho)\,(c - du) = \rho c \tag{9}$$

Neglecting second order differentials again

$$c\,d\rho = \rho\,du \tag{10}$$

Eliminating du between eq. 8 and eq.10, then rearranging

$$c^2 = \left(\frac{dP}{d\rho}\right)_S \tag{11}$$

Returning to the concepts of the canonical ensemble, the average ensemble energy in terms of the partion function is given by

$$\bar{E} = kT^2 \left(\frac{\partial \ln Q(N,V,T,)}{\partial T}\right)_{N,V} \qquad (12)$$

The partition function for an entire N particle system can be written in terms of the individual particle functions, q(V,T)

$$Q(N,V,T) = \frac{[q(V,T)]^N}{N!}$$

If the total Hamiltonian for the particles can be written as the summation of the Hamiltonians for the various degrees of freedoms within the particles, then the total partition function for the individual particles can be written as the product of the partition functions for the various degrees of freedoms within the particles, i.e., the Born-Oppenheimer approximation.

In the case of a momotomic gas

$$q(V,T) = q_{trans}\, q_{elect}\, q_{nuc}$$

and in the case of a diatomic gas

$$q(V,T) = q_{trans}\, q_{elect}\, q_{nuc}\, q_{rot}\, q_{vib}$$

The nuclear and electronic partition functions are usually set equal to unity, since the temperature must be very high to populate the excited levels under equilibrium conditions. A temperature on the order of 10^4 °K is required for the electronic levels and a temperature on the order of 10^{11} °K is required for the nuclear levels.

The translational energy levels are given by

$$E_i = 1/2\ m_i\ v_i^2$$

For a sufficiently large volume of particles the summation in the partition function can be transformed into an integral. The degeneracy of the translational energy differential elements is found to be

$$g(E) = \frac{4\pi V (2m^3)^{1/2} E^{1/2}}{h^3}$$

The translational partition function is then

$$q_{trans} = \frac{(2\pi mkT)^{3/2} V}{h^3}$$

The rotational energy levels for a rigid rotor are given by

$$E_J = \frac{\hbar^2}{2I} J(J+1)$$

where I is the moment of inertia of the molecule. The degeneracy of the rotational energy levels is 2J+1. For sufficiently high temperatures or small energy level spacings, the summation in the partition function can be transformed into an integral. The partition function is found to be

$$q_{rot} = \frac{T}{\theta_{rot}}$$

where θ_{rot} is the characteristic temperature of rotation and is given by

$$\theta_{rot} = \frac{\hbar^2}{2kI}$$

The vibrational energy levels of the harmonic oscillator are given by

$$E_v = h\upsilon\,(v + 1/2)$$

$$= \hbar\omega\,(v + 1/2)$$

The vibrational energy levels are non-degenerate. For sufficiently high temperatures, the summation in the partition function can be replaced by an integral. The partition function is found to be

$$q_{vib} = \frac{T}{\theta_{vib}}$$

where θ_{vib} is the characteristic temperature of vibration and is given by

$$\theta_{vib} = \frac{\hbar\omega}{k}$$

For a momotomic gas, the thermodynamic energy has only the contribution from the translation partition function

$$E_{trans} = kT^2 \left(\frac{\partial \ln Q_{trans}}{\partial T}\right)_{N,V}$$

$$= \frac{3}{2}\ NkT$$

For a diatomic gas, the thermodynamic energy may have additional contributions from the vibrational and rotational partition functions. For temperatures on the order of 10^2 °K, the rotational pattern function makes its full contribution.

$$E_{rot} = kT^2 \left(\frac{\partial \ln Q_{rot}}{\partial T}\right)_{N,V}$$

$$= NkT$$

For temperatures on the order of 10^3 °K, the translational partition function makes its full contribution.

$$E_{vib} = kT^2 \left(\frac{\partial \ln Q_{vib}}{\partial T}\right)_{N,V}$$

$$= NkT$$

The total energy is then the summation of the various contributions

$$E = E_{trans} + E_{rot} + E_{vib}$$

The product Nk can be written in terms of the gas constant to express the energy in terms of other units.

$$Nk = n\mathcal{R} = mR$$

The total energy in terms of the thermodynamic integral energy is then

$$E = nU = mU$$

The definitions of the specific heat give

$$C_v = \left(\frac{dU}{dT}\right)_V \tag{13}$$

$$C_p = \left(\frac{dU}{dT}\right)_p \tag{14}$$

For an ideal gas

$$PV = RT \tag{15}$$

$$dH = C_p\, dT \tag{16}$$

$$dU = C_v\, dT \tag{17}$$

Substituting eq. 15 into eq. 3

$$H = U + RT \tag{18}$$

Taking the derivative

$$DH = DU + R\, dT \tag{19}$$

Substituting for dH and dU from eqs. 16 and 17

$$C_p\, dT = C_v\, dT + R\, dT$$

Dividing by dT

$$R = C_p - C_v \tag{20}$$

The ratio of the specific heats is defined as γ

$$\gamma = \frac{C_p}{C_v} \tag{21}$$

Taking the derivative of eq. 3

$$dU = dQ - dW \tag{22}$$

Assuming an adiabatic case, $dQ = 0$

$$dU = - dW$$

Substituting eq. 17 for dU and eq. 6 for dW

$$C_v \, dT = - P \, dV \tag{23}$$

Taking the derivative of eq. 15

$$P \, dV + V \, dP = R \, dT \tag{24}$$

Eliminating dT from eqs. 23 and 24, and rearranging

$$V \, dP = - \left(\frac{R}{C_v} + 1 \right) P \, dV \tag{25}$$

From eq. 20

$$\frac{R}{C_v} + 1 = \gamma$$

Eq. 25 becomes

$$VdP = - \gamma P dV$$

Integrating

$$\ln P = - \gamma \ln V + \text{constant}$$

Rearranging

$$P V^{\gamma} = \text{constant}$$

Or

$$\frac{P}{\rho^{\gamma}} = \text{constant} \tag{26}$$

Taking the logarithum

$$\ln P - \gamma \ln \rho = \text{constant}$$

Taking the derivative

$$\frac{dP}{P} = \frac{\gamma d\rho}{\rho}$$

Rearranging

$$\frac{dP}{d\rho} = \frac{\gamma P}{P}$$

$$= \gamma PV$$

Recalling eq. 15

$$\frac{dP}{d\rho} = \gamma RT \qquad (27)$$

Since this development utilized the assumptions that the process was reversible, adiabatic, and therefore isentropic

$$W = W_{rev}$$

$$dQ = dQ_{rev} = 0$$

$$dS = 0$$

Eq. 27 can be written

$$\left(\frac{\partial P}{\partial \rho}\right)_S = \gamma RT \qquad (28)$$

Substituting eq. 28 into eq. 11

$$c^2 = \gamma RT$$

Or

$$c = (\gamma RT)^{\frac{1}{2}} \tag{29}$$

Now consider the flow of a compressible fluid through a nozzle. Since the flow through a nozzle is usually very fast, it can be assumed that there is negligible heat transfer. Therefore the flow can be assumed to be adiabatic. Also, nozzles can be designed so that they operate reversibly. Therefore, flow through nozzles can be assumed to be isentropic.

Figure 23 illustrates the flow of a compressible fluid through a converging-diverging nozzle. The section of the nozzle with the smallest cross-sectional area is the throat.

A steady state energy balance around the inlet of the nozzle can be written

$$H_{in} + 1/2\ u_{in}^2 = H + 1/2\ u^2$$

where H and u are for an arbitrary position in the nozzle.

For most nozzles, the inlet velocity can be neglected

$$u >> u_{in}$$

So that

$$H - H_{in} = - 1/2\ u^2$$

Taking the derivative

$$dH = - u\ du \tag{30}$$

Recalling the thermodynamic relation eq. 8

$$dH = T\ dS + V\ dP$$

Since the system is isentropic

$$dH = V\ dP \tag{31}$$

Eliminating dH between eqs. 30 and 31

$$V\ dP = - u\ du$$

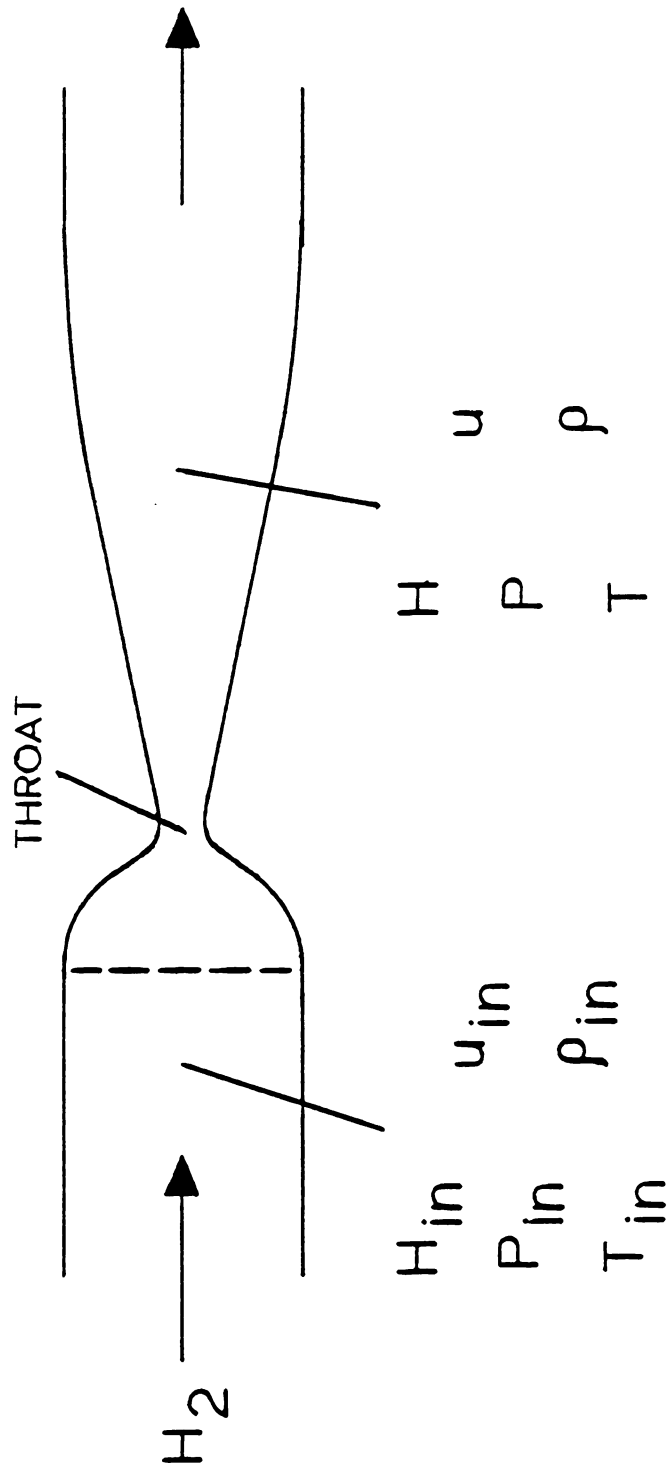

Figure 23. Compressible fluid flow through a converging-diverging nozzle.

Or

$$\frac{dP}{du} = \frac{-u}{V} \tag{32}$$

Which states that the pressure always decreases for an accelerating flow and increases for a decelerating flow.

$$\frac{dP}{du} < 0$$

A steady state mass balance around the inlet of the nozzle can be written

$$\rho_{in} A_{in} u_{in} = \rho A u = \text{constant}$$

Taking the derivative

$$Aud\rho + \rho Adu + \rho udA = 0$$

Dividing by ρuA

$$\frac{d\rho}{\rho} + \frac{du}{u} + \frac{dA}{A} = 0$$

Substituting eq. 32 for du

$$\frac{d\rho}{\rho} + \frac{dA}{A} - \frac{V\, dP}{u^2} = 0$$

Rearranging

$$\frac{dA}{A} = \frac{dP}{\rho}\left(\frac{1}{u^2} - \frac{d\rho}{dP}\right)$$

Substituting eq. 11 for $\frac{d\rho}{dP}$

$$\frac{dA}{A} = \frac{dP}{\rho}\left(\frac{1}{u^2} - \frac{1}{c^2}\right)$$

Or

$$\frac{dA}{A} = \frac{dP}{\rho u^2}\left(1 - \frac{u^2}{c^2}\right)$$

The Mach number, M, is defined as

$$M = \frac{u}{c}$$

So that

$$\frac{dA}{A} = \frac{(1 - M^2)}{\rho u^2} dP \qquad (33)$$

Eq. 33 shows that:

1) for subsonic flow ($M < 1$)

$$\frac{dA}{dP} > 0 \; ; \; \frac{dA}{du} < 0$$

2) For supersonic flow ($M > 1$)

$$\frac{dA}{dP} < 0 \; ; \; \frac{dA}{du} > 0$$

3) for sonic flow ($M = 1$)

$$\frac{dA}{dP} = \frac{dA}{du} = 0$$

these results are shown in Figure 24.

These results show that the cross-sectional area goes through a minimum at the sonic velocity ($M = 1$). For a fixed mass flow rate, w, a minimum in the cross-sectional area, A, corresponds to a maximum in the velocity, u. And since this ocurrs at Mach 1, the maximum velocity that can be obtained in the throat of a nozzle is the velocity of sound at the throat conditions.

This study is concerned only with the converging portion of a converging-diverging nozzle operated under "choked" flow conditions. "Choked" flow implies that the mass flow rate throught the nozzle is determined by the cross-sectional area of the throat and the condi-

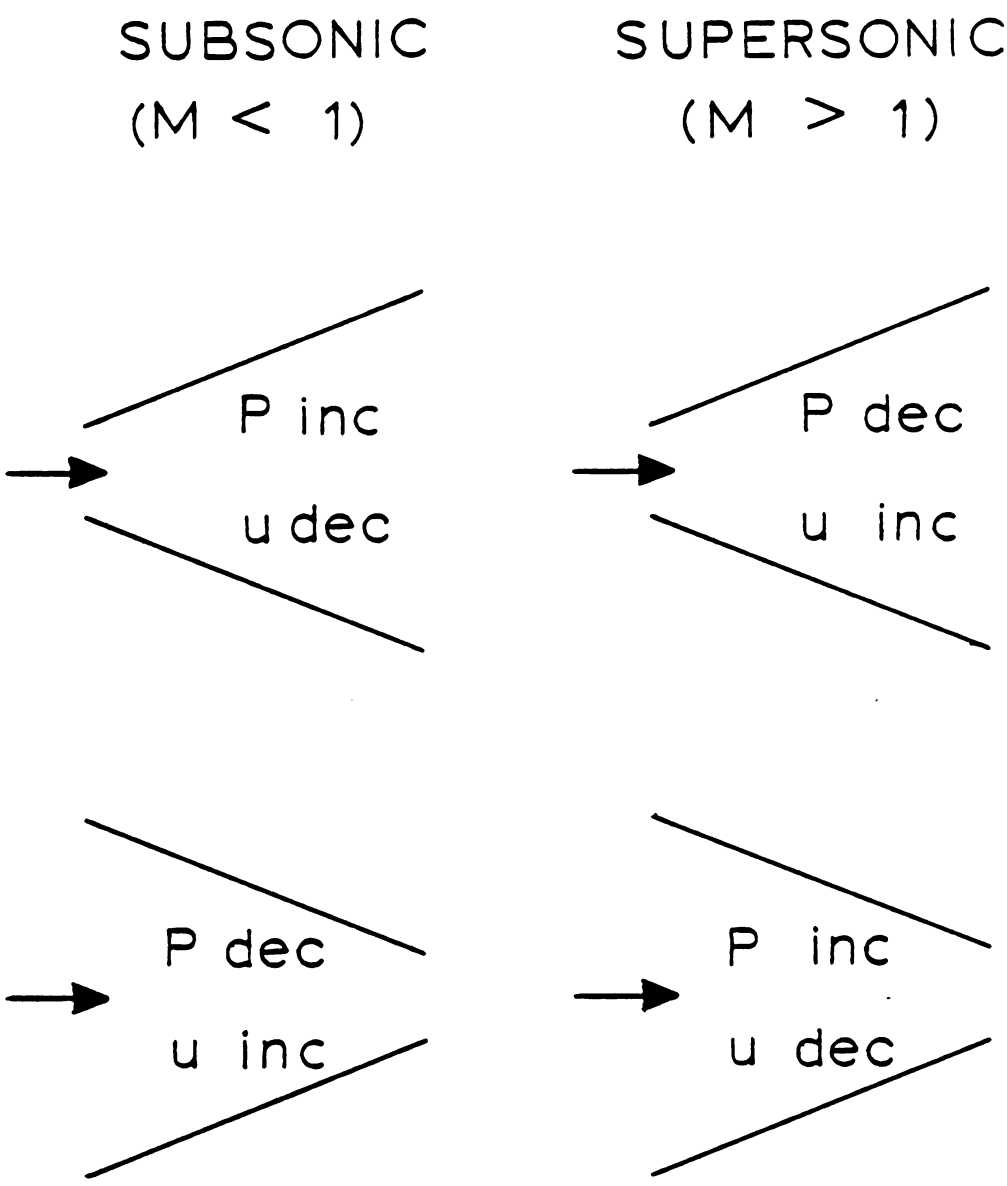

Figure 24. Effect of cross-sectional area on supersonic and subsonic flow.

tions of the fluid upstream of the throat. The flow rate is independent of the conditions of the fluid downstream of the nozzle. Sonic flow is maintained in the throat.

The conditions of the fluid upstream of the nozzle become stagnation conditions

$$u_{in} = 0$$

$$P_{in} = P_o$$

$$H_{in} = H_o$$

$$T_{in} = T_o$$

$$\rho_{in} = \rho_o$$

The steady state mass balance around the inlet of the nozzle can be written

$$\frac{w}{A} = \rho u \tag{34}$$

Recalling eq. 15

$$PV = RT$$

Written in terms of ρ

$$\frac{P}{\rho} = RT$$

Rearranging

$$\rho = \frac{P}{RT} \tag{35}$$

Substituting for ρ in eq. 34

$$\frac{w}{A} = \frac{Pu}{RT}$$

Expressing u in terms of M

$$\frac{w}{A} = \frac{PMc}{RT}$$

Substituting eq. 29 for c

$$\frac{w}{A} = \left(\frac{\gamma}{RT}\right)^{\frac{1}{2}} P M \qquad (36)$$

The steady state energy balance around the inlet of the nozzle can be written

$$H_o = H + 1/2\ u^2 \qquad (37)$$

Assuming an ideal gas and utilizing eq. 14

$$C_p (T_o - T) = 1/2\ u^2 \qquad (38)$$

Recalling eqs. 20 and 21

$$C_p - C_v = R$$

$$\frac{C_p}{C_v} = \gamma$$

Eliminating C_v between eqs. 20 and 21

$$\frac{C_p}{C_p - R} = \gamma$$

Rearranging

$$C_p = \frac{\gamma R}{\gamma - 1}$$

Substituting for C_p into eq. 38

$$\frac{\gamma R}{\gamma - 1} (T_o - T) = 1/2\ u^2$$

Rearranging

$$\frac{T_o}{T} = 1 + \frac{u^2 (\gamma - 1)}{2\gamma RT}$$

Substituting eq 29 for c

$$\frac{T_o}{T} = 1 + \frac{(\gamma - 1)\ u^2}{2c^2}$$

$$\frac{T_o}{T} = 1 + \left(\frac{\gamma-1}{2}\right) M^2$$

Or

$$T = \frac{T_o}{1 + \left(\frac{\gamma-1}{2}\right) M^2} \tag{39}$$

Recalling eq. 26

$$\frac{P}{\rho^\gamma} = \text{constant}$$

Which can be written

$$\frac{P}{P_o} = \left(\frac{\rho}{\rho_o}\right)^\gamma$$

Substituting eq. 35 for ρ and rearranging

$$\frac{P}{P_o} = \left[\frac{T}{T_o}\right]^{\left(\frac{\gamma}{\gamma-1}\right)}$$

Substituting eq. 39 for T and rearranging

$$\frac{P}{P_o} = \left[1 + \frac{\gamma-1}{2} M^2\right]^{\left(\frac{-\gamma}{\gamma-1}\right)} \tag{40}$$

Substituting eq. 40 for P and eq. 39 for T into eq. 36

$$\frac{w}{A} = \left(\frac{\gamma}{RT_o}\right)^{\frac{1}{2}} MP_o \left[1 + \frac{\gamma-1}{2} M^2\right]^{\left(\frac{-(\gamma+1)}{2(\gamma-1)}\right)} \tag{41}$$

Taking the derivative with respect to M

$$\frac{d\left(\frac{w}{A}\right)}{dM} = \left(\frac{T}{RT_o}\right)^{\frac{1}{2}} P_o \frac{1-M^2}{\left(\frac{\gamma+1}{2(\gamma-1)}+1\right)\left[1+\frac{\gamma-1}{2}M^2\right]}$$

$$= 0 \qquad \text{for } M = 1$$

Which is the identical result obtained previously. Therefore, setting $M = 1$ in eq. 41, gives the maximum mass flow rate per unit area obtainable through a nozzle.

$$\left(\frac{w}{A}\right)_{max} = \left(\frac{\gamma}{RT_o}\right)^{\frac{1}{2}} P_o \left(\frac{2}{\gamma+1}\right)^{\left(\frac{\gamma+1}{2(\gamma-1)}\right)}$$

$$= \left[\frac{\gamma}{RT_o}\left(\frac{2}{\gamma+1}\right)^{\left(\frac{\gamma+1}{\gamma-1}\right)}\right]^{1/2} P_o$$

Since $R = \mathcal{R}M$

$$\left(\frac{w}{A}\right)_{max} = \left(\frac{M\gamma}{\mathcal{R}T_o}\right)^{\frac{1}{2}} P_o \left[\frac{2}{\gamma+1}\right]^{\left(\frac{\gamma+1}{2(\gamma-1)}\right)} \tag{42}$$

II. Calculations and Results

The experimental flow system was operated under "choked" flow conditions. This was verified by the fact that the pressure upstream of the nozzle was three orders of magnitude greater than the downstream pressure, and that small changes in the downstream pressure did not affect the mass flow rate through the nozzle or the upstream pressure.

Eq. 42 was utilized in calculating the gas dynamic temperature. The pressure upstream of the nozzle was measured at room temperature conditions (zero absorbed power and plasma absent) for a series of mass flow rates. Then the upstream pressure was measured at steady state plasma conditions for the same mass flow rates.

Since the upstream pressures were measured at the same mass flow rates and the cross-sectional area of the nozzle was constant

$$\left(\frac{w}{A}\right)_{\substack{\text{room}\\\text{temp}}} = \left(\frac{w}{A}\right)_{\text{plasma}}$$

Substituting eq. 42 for w/A

$$\left[\left(\frac{M\gamma}{\mathcal{R}T_o}\right)^{\frac{1}{2}}\left[\frac{2}{\gamma+1}\right]^{\left(\frac{\gamma+1}{2(\gamma-1)}\right)}P_o\right]_{\substack{\text{room}\\\text{temp}}} = \left[\left(\frac{M\gamma}{\mathcal{R}T_o}\right)^{\frac{1}{2}}\left[\frac{2}{\gamma+1}\right]^{\left(\frac{\gamma+1}{2(\gamma-1)}\right)}P_o\right]_{\text{plasma}} \tag{43}$$

At room temperature conditions, the constants, stagnation pressure and temperature are denoted

$$T_o = T$$

$$P_o = P$$

$$\gamma = \gamma$$

$$M = M$$

At steady state plasma conditions, the constants, stagnation pressure and temperature are denoted

$$T_o = T_{gd}$$

$$P_o = P^*$$

$$\gamma = \gamma^*$$

$$M = M^*$$

Since the quantity desired is the upstream steady state plasma temperature, i.e., the gas dynamic temperature, eq. 43 is rewritten

$$T_{gd} = T \left(\frac{P^*}{P}\right)^2 \frac{M^* \gamma^* \left[\frac{2}{\gamma^*+1}\right]^{\left(\frac{\gamma^*+1}{\gamma^*-1}\right)}}{M \gamma \left[\frac{2}{\gamma+1}\right]^{\left(\frac{\gamma+1}{\gamma-1}\right)}} \tag{44}$$

At room temperature conditions, the gas consists of strictly molecular hydrogen. The molecular weight is

$$M = M_{H_2}$$
$$= 2 \tag{45}$$

The specific heats are

$$C_p = C_{p_{H_2}}$$
$$C_v = C_{v_{H_2}}$$

The ratio of the specific heats is then

$$\gamma = \frac{C_{p_{H_2}}}{C_{v_{H_2}}}$$

Which can be rewritten in terms of the heat capacities

$$\gamma = \frac{C_{p_{H_2}}}{C_{v_{H_2}}} \tag{46}$$

At steady state plasma conditions, however, some of the molecular hydrogen has been dissociated into atomic hydrogen. The degree to which dissociation occurs in the plasma is characterized by the conversion, z, which is defined as the molar fraction of the molecular hydrogen that dissociates into atomic hydrogen. The conversion at an arbitrary position in the plasma and its relationship to the mole

fractions, x_i, are shown in Table 5. From the mole fractions, the effective molecular weight of the plasma can be found in terms of the conversion

$$M^* = \sum_i M_i \, x_i$$

$$= \frac{2z}{1+z} M_H + \frac{1-z}{1+z} M_{H_2}$$

Since

$$M_H = 1$$

$$M_{H_2} = 2$$

The effective molecular weight becomes

$$M^* = \frac{2}{1+z} \tag{47}$$

The mass fractions, x_i, can be written in terms of the mole fractions.

$$x_i = \frac{M_i \, x_i}{\sum_j M_j \, x_j}$$

The mass fractions for atomic and molecular hydrogen can be rewritten in terms of the conversion

$$x_H = \frac{\frac{2z}{1+z} M_H}{\frac{2z}{1+z} M_H + \frac{1-z}{1+z} M_{H_2}}$$

$$x_{H_2} = \frac{\frac{1-z}{1+z} M_{H_2}}{\frac{2z}{1+z} M_H + \frac{1-z}{1+z} M_{H_2}}$$

From the mass fractions, the specific heats of the plasma can be found in terms of the conversion.

TABLE 5
STOICHIOMETRIC TABLE

Species	Flow in (moles)	Flow out (moles)	x Mole Fraction	x Mass Fraction
H	0	$2z\ F_o$	$\frac{2z}{1+z}$	z
H_2	F_o	$(1-z)\ F_o$	$\frac{1-z}{1+z}$	1 - z
Total	F_o	$(1+z)\ F_o$	1	1

where z is the conversion, i.e., the fraction of moles of H_2 that is dissociated into H.

$$C^* = \sum_i C_i x_i$$

$$= \frac{\frac{2z}{1+z} C_H M_H + \frac{1-z}{1+z} C_{H_2} M_{H_2}}{\frac{2z}{1+z} M_H + \frac{1-z}{1+z} M_{H_2}}$$

The ratio of the specific heats is then

$$\gamma^* = \frac{2z\, C_{p_H} M_H + (1-z)\, C_{p_{H_2}} M_{H_2}}{2z\, C_{v_H} M_H + (1-z)\, C_{v_{H_2}} M_{H_2}}$$

which can be rewritten in terms of the converison and heat capacities

$$\gamma^* = \frac{2z\, \mathcal{C}_{p_H} + (1-z)\, \mathcal{C}_{p_{H_2}}}{2z\, \mathcal{C}_{v_H} + (1-z)\, \mathcal{C}_{v_{H_2}}} \tag{48}$$

Since atomic hydrogen is a monatomic gas, the internal energy is purely translation. Assuming an ideal gas, the heat capacities for atomic hydrogen are then

$$\mathcal{C}_{p_H} = \frac{5}{2} R$$

$$\mathcal{C}_{v_H} = \frac{3}{2} R$$

Since molecular hydrogen is a diatomic gas, the internal energy may have contributions from the rotational and vibrational energies in addition to the translational energy. The characteristic temperatures of rotation and vibration for molecular hydrogen are

$$\theta_{rot} \sim 85\ ^\circ K$$

$$\theta_{vib} \sim 6200\ ^\circ K$$

For the temperatures generated in this experiment (~1000 °K), the internal energy for molecular hydrogen will have a full contribution from the rotational energy and no contribution from the vibrational energy (Alonzo, 1968).

Assuming an ideal gas, the heat capacities for molecular hydrogen are then

$$C_{p_{H_2}} = \frac{7}{2} R$$

$$C_{v_{H_2}} = \frac{5}{2} R$$

Substituting these values for the heat capacities into eqs. 46 and 48, the ratios of the specific heats in terms of the conversion become

$$\gamma = \frac{7}{5} \tag{49}$$

$$\gamma^* = \frac{3z+7}{z+5} \tag{50}$$

Substituting eqs. 45, 47, 49, and 50 into eq. 44, the equation for the gas dynamic temperature becomes

$$T_{gd} = T \left(\frac{P^*}{P}\right)^2 \left(\frac{2.13285}{1+z}\right) \left(\frac{3z+7}{z+5}\right) \left(\frac{z+5}{2(z+3)}\right)^{\left(\frac{2(z+3)}{z+1}\right)}$$

Unfortunately, the experimental apparatus did not allow for the determination of the conversion. Previous work indicates that the conversion generally increases with absorbed power and flow rate, while it decreases with increasing pressure. For similar conditions the conversion was shown to range from 5% to 20% (Chapman, 1982).

Figure 25 shows the effect of the conversion on the gas dynamic temperature. Figures 26 through 29 show the gas dynamic temperature as a function of absorbed power for various conversions , at given flow rates (pressures). As can be seen from the figures, the gas dymanic temperature generally increases with increasing flow rate (pressure) and absorbed power.

Since the conversion is not known, the error of the gas dynamic temperature measurement can not be calculated. The conversion could be measured spectroscopically or estimated by constructing a mathematical model. However, assuming conversions of 0% and 100% for the gas dynamic temperature calculations provide useful upper and lower bounds respectively for the gas dynamic temperature.

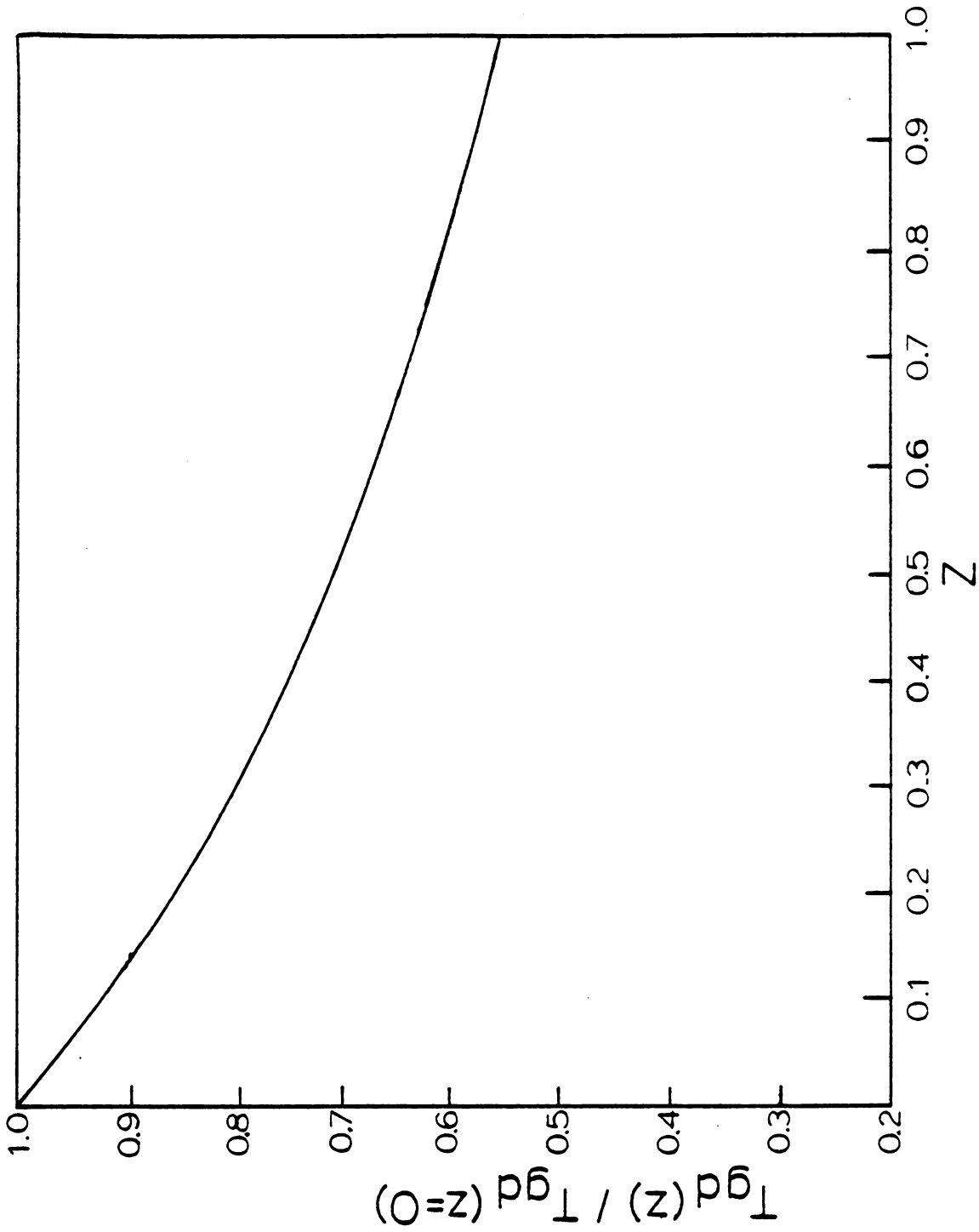

Figure 25. Gas dynamic temperature as a function of conversion.

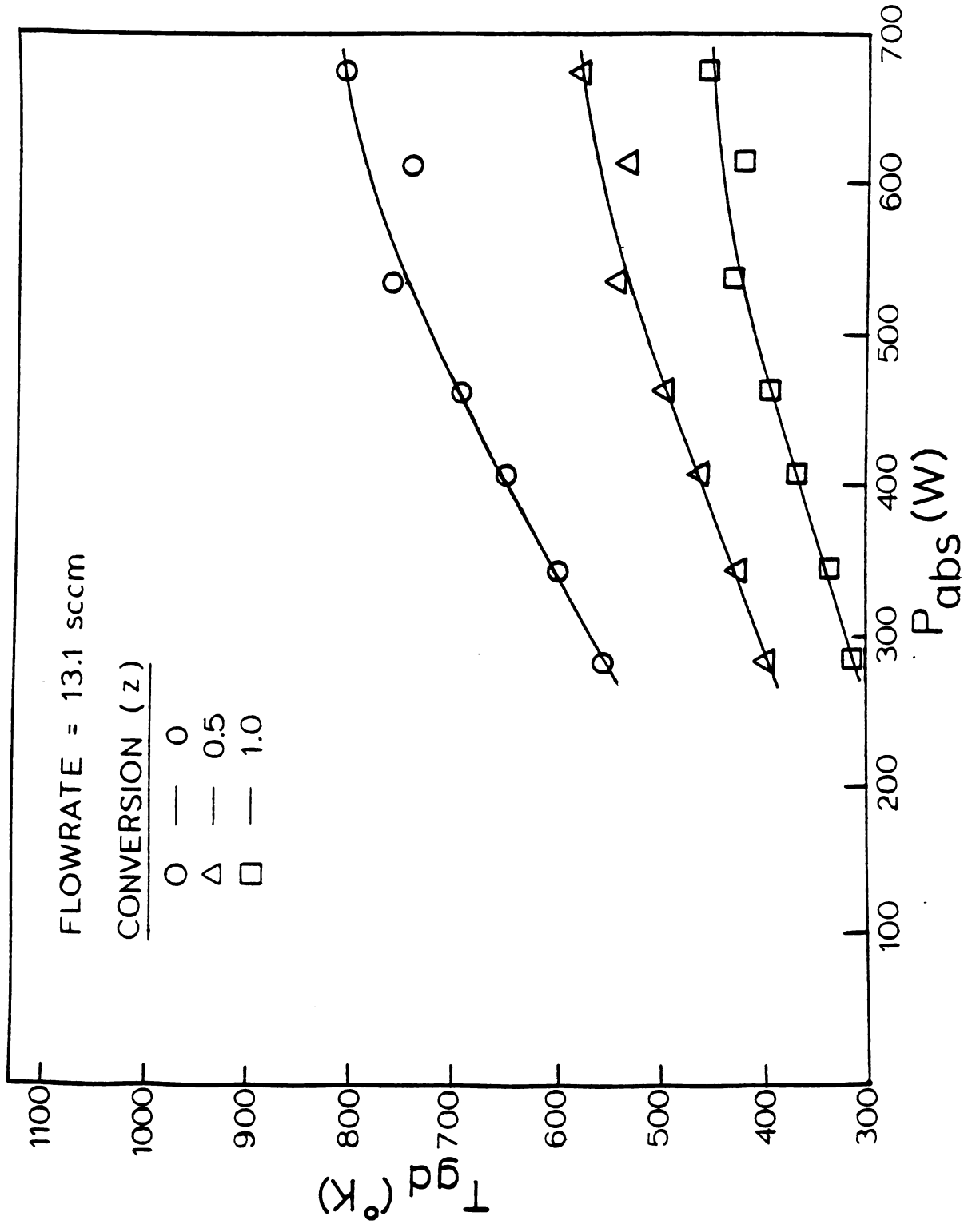

Figure 26. Gas dynamic temperature as a function of absorbed power for various conversions at 13.1 sccm.

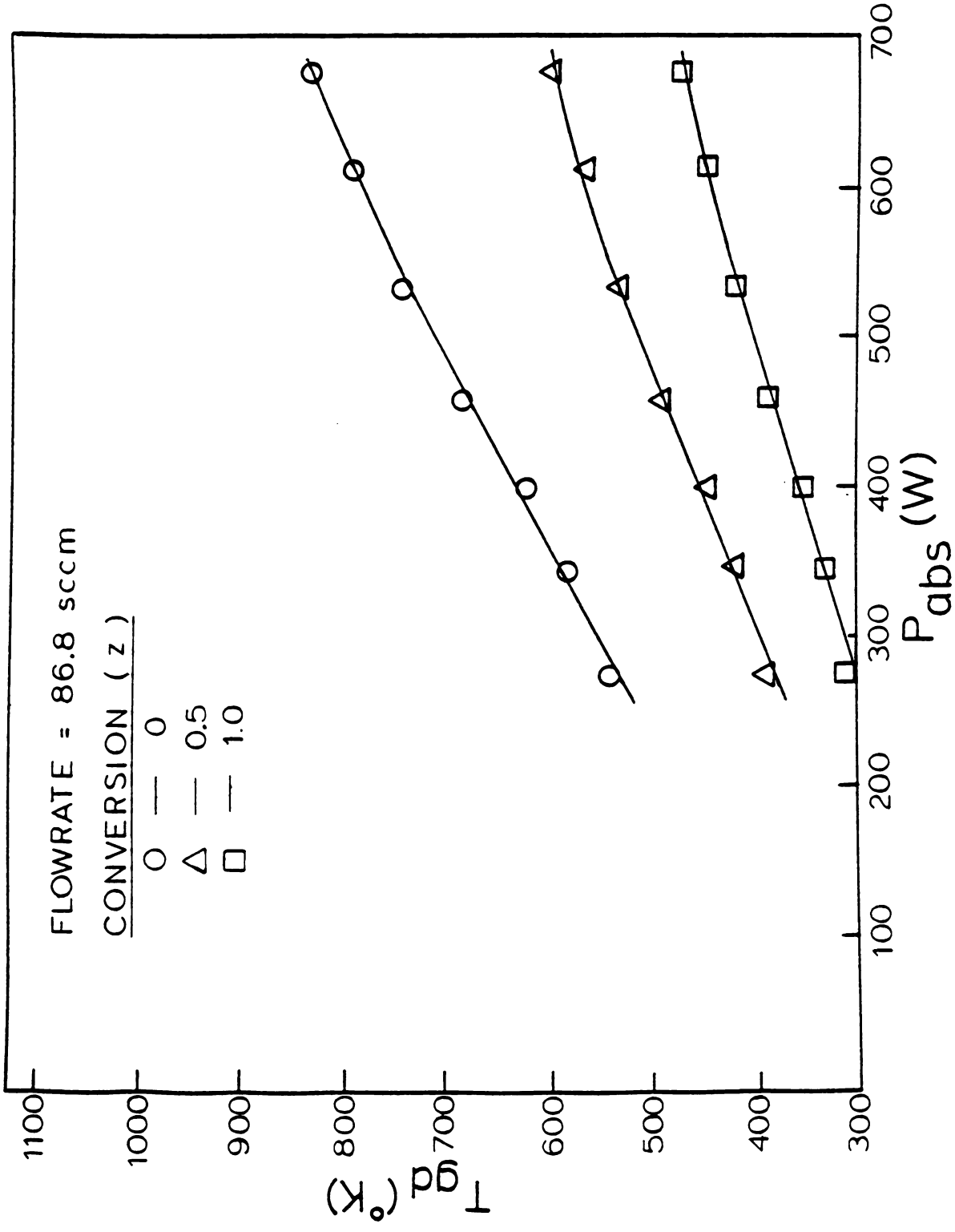

Figure 27. Gas dynamic temperature as a function of absorbed power for various conversions at 86.8 sccm.

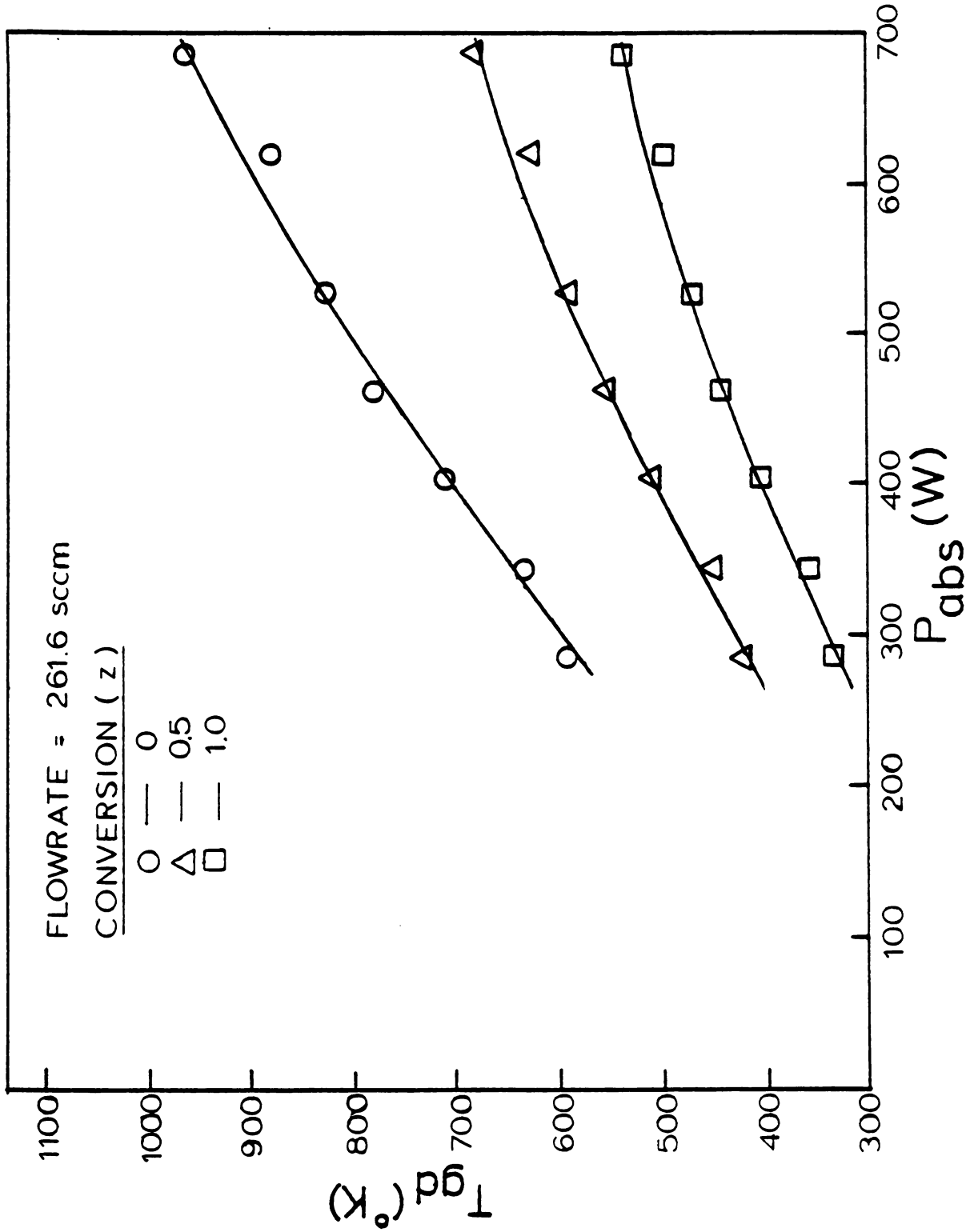

Figure 28. Gas dynamic temperature as a function of absorbed power for various conversions at 261.6 sccm.

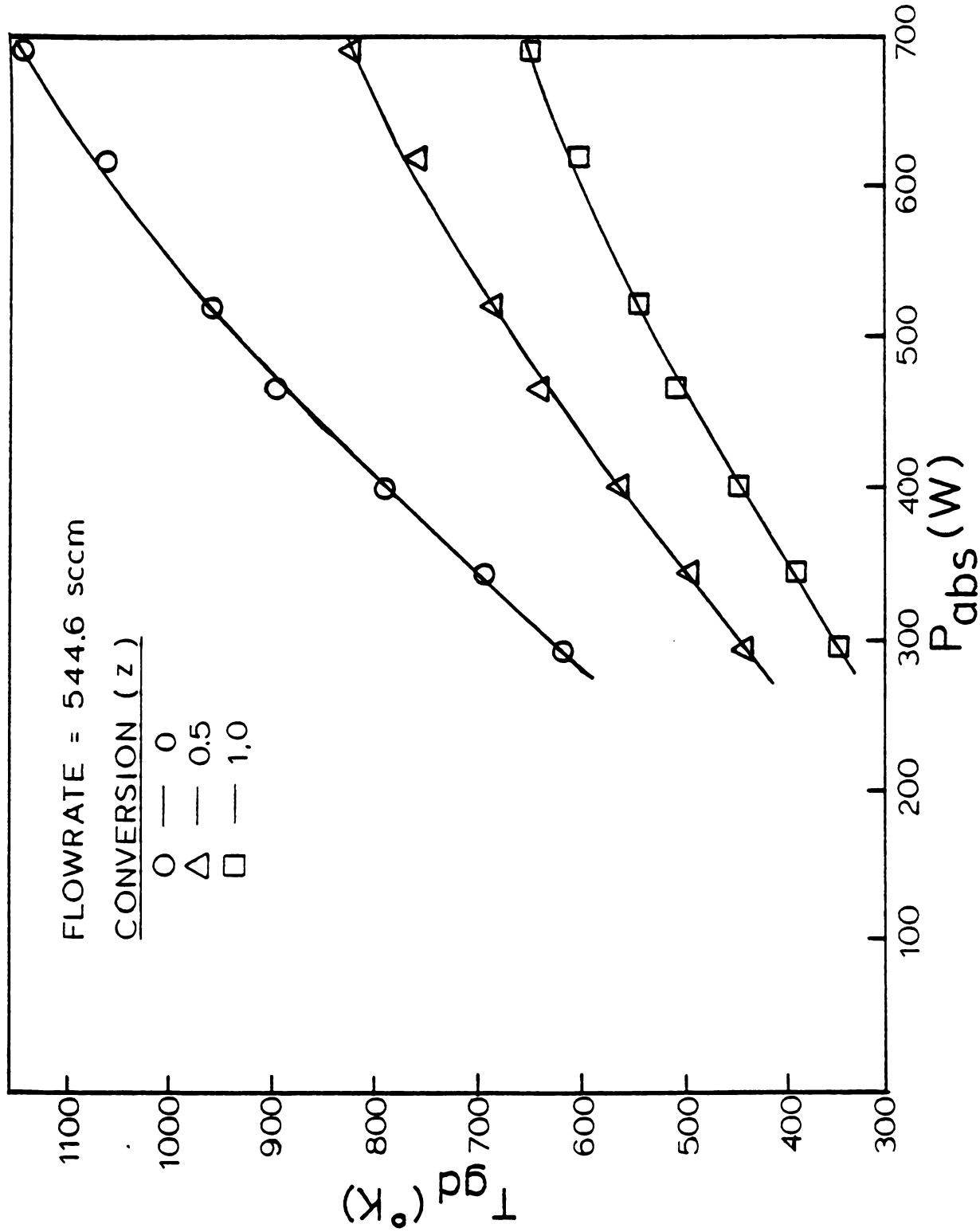

Figure 29. Gas dynamic temperature as a function of absorbed power for various conversions at 544.6 sccm.

ENERGY TRANSFER

Since the electrothermal propulsion concept involves the conversion of electromagnetic energy into gas kinetic energy, it is important to be able to determine the effectiveness of that energy interchange. The energy input of the system is the power absorbed by the plasma cavity system supplied by the microwave power source. The energy outputs of the system are the increase in the total energy of the gas as it flows through the system, the power absorbed by the air cooling of the discharge tube, the power absorbed by the water cooling of the resonant cavity, and the radiation that escapes the system. A steady state energy balance around the system can be written

$$P_{abs} = P_{gas} + P_{air} + P_{water} + P_{rad}$$

For the purposes of this study, the last two energy outputs were neglected. Previous work has shown that an optimally tuned resonant cavity absorbs only 1-2% of the power absorbed by the plasma cavity system (Rogers, 1982). Also the power contained in the escaping radiation was extremely small. The energy balance then becomes

$$P_{abs} = P_{gas} + P_{air}$$

The power absorbed by the plasma cavity system was measured by the directional couplers and power meters. The power absorbed by the cooling air was determined by its temperature rise. The cooling air was delivered to the system at a constant temperature, T_{in}, and mass flow rate, w_{air}.

$$T_{in} = 292°K$$

$$w_{air} = 3.7 \text{ g/sec}$$

The outlet temperature of the cooling air was measured by an iron-

constant thermocouple. The power absorbed by the cooling air was then calculated for a given plasma gas flow rate (pressure) as a function of absorbed power.

$$P_{air}\ (W) = \int_{T_{in}}^{T_{out}} w_{air}\ C_{p_{air}}\ dT$$

The specific heat of the cooling air is (Himmelblau, 1974)

$$C_{p_{air}}\ (\frac{J}{g\,^{\circ}K}) = a + bT + cT^2 + dT^3$$

where

$a = 1.0786$

$b = 7.5469 \times 10^{-5}$

$c = 1.8430 \times 10^{-7}$

$d = -7.5453 \times 10^{-11}$

The power absorbed the gas as it flows through the system can then be calculated by the difference

$$P_{gas} = P_{abs} - P_{air}$$

The power absorbed by the gas was found to be independent of the flowrate (pressure) of the plasma. The percentage of the power absorbed by the plasma system which remains in the gas as it flows through the system is denoted by $\%P_{gas}$.

$$\%P_{gas} = 100 \times \frac{P_{gas}}{P_{abs}}$$

Figure 30 shows $\%P_{gas}$ as a function of absorbed power. As can be seen from the figure, $\%P_{gas}$ increases with increasing absorbed power.

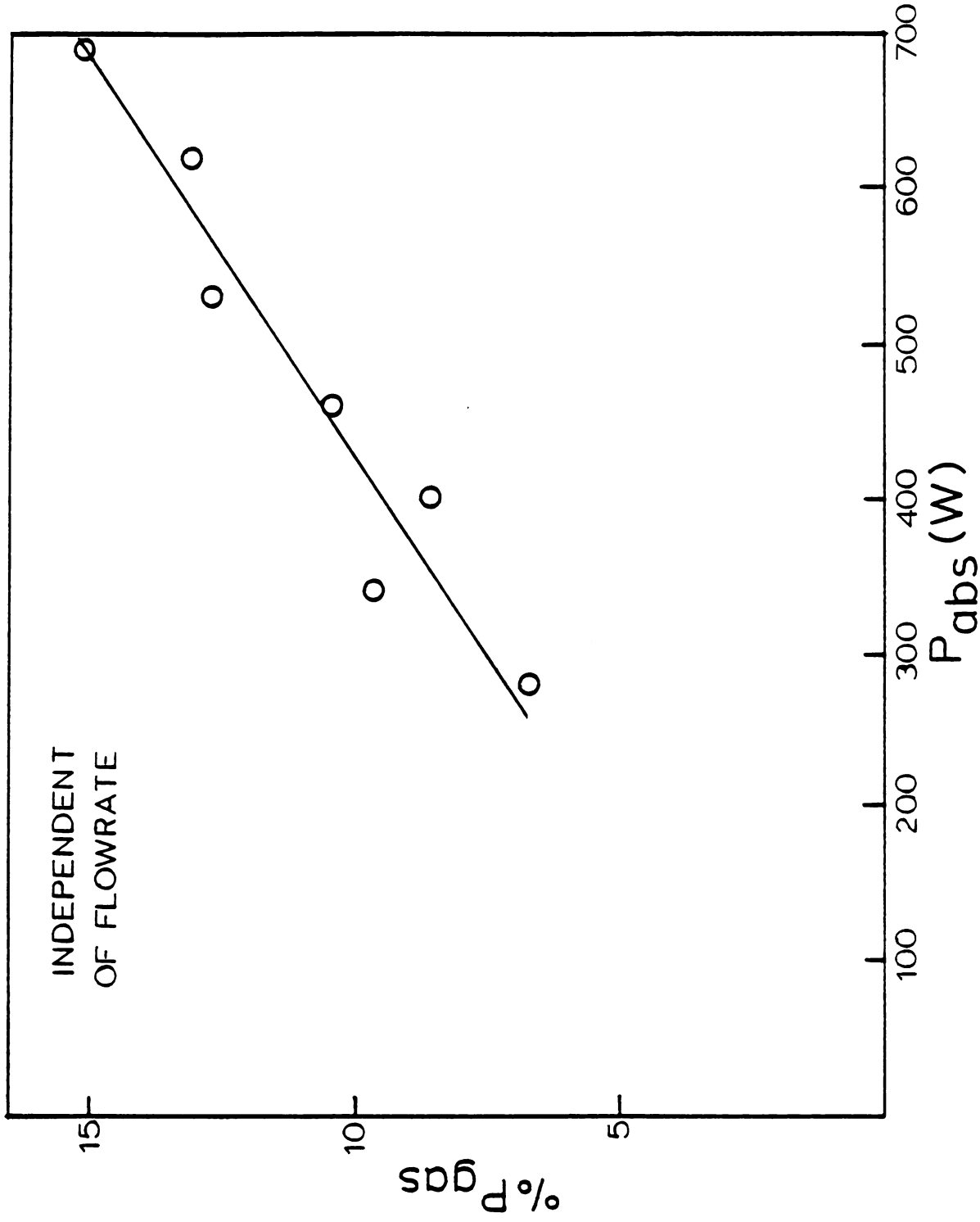

Figure 30. Percent power absorbed by the plasma system which remains in the gas as a function of absorbed power.

The cooling air does not absorb its power directly. Since atmospheric air is transparent of microwave radiation, all of the power absorbed by the plasma cavity system, minus the power absorbed by the cooling water, is first absorbed by the plasma gas. The power that does not remain in the gas is either radiated, or transferred to the discharge tube wall and subsequently carried away by the cooling air.

Though these results are obtained from a simplistic energy balance, they provide a useful upper bound to the percentage of the power applied to the system that is ultimately transferred to the flowing gas for these experimental conditions.

CONCLUSION

Gas temperature measurements have been obtained for hydrogen in a flowing microwave plasma. These temperatures were found to vary from 700 to 1000 °K for absorbed powers ranging from 280 to 700 W, pressures ranging from 1.0 to 10.0 torr, and flow rates ranging from 10 to 500 μmoles/sec. Rotational temperatures were determined from spectroscopic measruements of the emission spectra in the visible region. Gas dynamical temperatures were determined from pressure measurements upstream of the nozzle operated under "choked" flow conditions. These temperatures had very good agreement and were found to increase with increasing absorbed power and flowrate (with pressure coupled to flow rate).

The purpose of this study was to determine the usefulness of the spectroscopic technique in measuring the gas temperature. The gas dynamic method was utilized to obtain an independent gas temperature measurement for comparison. The spectroscopic method proved to be very useful. It can be used under many operating conditions and configurations, with the advantage of being totally unperturbing to the system. In particular, the spectroscopic method can be used to obtain gas temperature measurements for plasmas where the pressure and flow rate are not coupled, and the effect of the pressure and flow rate on the gas temperature could be determined, independently of one another.

The assumption of thermal equilibrium of the rotational levels is an important one. Values for the characteristic temperatures of rotation and vibration, θ_{rot} and θ_{vib}, are 85 °K and 6200 °K, respec-

tively. This indicates that for the experimental laboratory plasmas with temperatures around 1000°K, the rotational energy levels can be assumed to be in thermal equilibrium while the vibrational energy levels can not. Alternatively, the populations of the rotational and vibrational energy levels can be calculated using the rigid rotor and harmonic oscillator approximations, respectively. These results also indicate that the rotational energy levels are in thermal equilibrium whereas the vibrational energy levels are not.

The four different electronic-vibronic transitions used in the calculations resulted in four consistently different sets of rotational temperatures. These differences were largest for the lower pressures (flow rates) and became negligible for the higher pressures (flow rates). This observation tends to suggest that the excited electronic and vibrational states are not in thermal equilibrium at the lower pressures while they may approach thermal equilibrium at the higher pressures. This notion is consistent with the fact that those states are excited by electron impact, and that the electrons in a microwave sustained plasma are not in thermal equilibrium with the rest of the plasma.

However, as the pressure increases, the collision frequency increases, bringing the excited states of the plasma species towards thermal equilibrium. The temperatures measured in this study are "bulk" temperature, i.e., temperatures that are spatially averaged over the entire plasma volume. Visual observation of the plasma emission shows quite readily that the plasma is not a homogenous medium. The plasma emission, and therefore some of its charac-

teristics, are dependent on the electromagnetic resonant mode of the plasma cavity. The spectroscopic technique can be refined with the implementation of lenses or optical fibers to obtain multidimensional temperature profiles of the plasma.

The error of the spectroscopc method was determined by the dark current noise of the photomultiplier tube and the plasma emission fluctuations resulting from the microwave power source instabilities. These limitations are due to the laboratory equipment and could be improved with higher quality equipment.

The error of the gas dynamic method was due to the uncertainty in the extent of dissociation present in the plasma. This error could be greatly reduced by the measurement or prediction of the extent of dissociation.

Recommendations for further work include:

1. Determine the effect of the pressure and flow rate on the gas temperature as independent variables.

2. Extend the ranges of the experimental variables to include lower absorbed power levels, higher gas flow rates, and both higher and lower pressures.

3. Study the effect of various cavity resonant modes, discharge tube diameters, configurations and surface coatings.

4. Enclose the system in a detailed, high resolution energy balance to determine energy distribution and transfer mechanisms of the system.

LIST OF REFERENCES

LIST OF REFERENCES

1. Alonso, M. and Finn, E., Fundamental University Physics, III. Quantum and Statistical Physics, Addison-Wesley, 1968.

2. Baker, H.D., Ryder, W., and Baker, N.H., Temperature Measurement in Engineering, Wiley, 1961.

3. Brown, S.C., Basic Data of Plasma Physics, MIT Press, 1966.

4. Chapman, R., Filpus, J., Morin, T., Snellenberger, R., Asmussen, J., Hawley, M., and Kerber, R., "Microwave Plasma Generation of Hydrogen Atoms for Rocket Propulsion," J. Spacecraft, Vol. 19, No. 6, 1982, p. 579.

5. Cherrington, B.E., Gaseous Electronics and Gas Lasers, Pergamon, 1979.

6. Dieke, G.H., "The Molecular Spectrum of Hydrogen and Its Isotopes," J. Mol. Spect., Vol. 2, 1958, p. 494.

7. Gaydon, A.G., The Spectroscopy of Flames, Wiley, 1954.

8. Hawkins, C.E. and Nakanishi, S., "Free Radical Propulsion Concept," NASA TM 81770, 1981.

9. Herzberg, G., Molecular Spectra and Molecular Structure, I., Spectra of Diatomic Molecules, Van Nostrand, 1950.

10. Himmelblau, D.M., Basic Principles and Calculations in Chemical Engineering, Prentice-Hall, 1974.

11. Jackson, J.D., Classical Electrodynamics, Wiley, 1975.

12. Krall, N. and Trivelpiece, A., Principles of Plasma Physics, McGraw-Hill, 1973.

13. Mallavarpu, R., "An Investigation of the Electromagnetic Behavior of a Microwave Plasma Source Over a Wide Range of Pressures and Flow Rates" Ph.D. Dissertation, Michigan State University, 1976.

14. McQuarrie, D., Statistical Mechanics, Harper and Row, 1973.

15. Meyer, S.C., Dta Analysisfor Scientists and Engineers, Wiley, 1975.

16. Richardson, O.W., Molecular Hydrogen and Its Spectrum, Yale, 1934.

17. Rogers, J.R., "Properties of Steady State, High Pressure, Argon Microwave Discharges," Ph.D. Dissertation, Michigan State University, 1982.

18. Schiff, L., Quantum Mechanics, McGraw-Hill, 1968.

19. Shapiro, A.H., The Dynamics and Thermodynamics of Compressible Fluid Flow, Vol. 1, Wiley, 1953.

20. Sharp, T.E., "Potential Energy Curves for Molecular Hydrogen and Its Ions," Atomic Data, Vol. 2, No. 2, 1971, p. 119.